ELSEVIER

Contents lists available at ScienceDirect

Journal of Food Engineering

journal homepage: www.elsevier.com/locate/jfoodeng





Convergence of Digital Twins and food drying technology: How to bring the next generation of dryers to life!?

Arman Arefi ^{a,*}, Carlos Vilas ^b, Mulugeta Admasu Delele ^{a,c}, Petra Foerst ^d, Sebastian Gruber ^d, Mohammad Kaveh ^e, Farhad Khoshnam ^{a,f}, Norhashila Hashim ^{g,h}, Maimunah Mohd Ali ^{i,j}, Saman Zohrabi ^k, Muhammad Tayyab ^{a,l}, Aditya Parmar ^{m,n}, Pramod Aradwad ^{a,o,p}, John Ndisya ^{a,q}, Waseem Amjad ^r, Majharulislam Babor ^a, Annika Mahn ^{a,l}, Barbara Sturm ^{a,l,**}

- ^a Leibniz Institute for Agricultural Engineering and Bioeconomy (ATB), Potsdam, Germany
- ^b Biosystems and Bioprocess Engineering Group, IIM-CSIC, c/ Eduardo Cabello, 6, 36208, Vigo, Spain
- ^c Faculty of Chemical and Food Engineering, Bahir Dar Institute of Technology, Bahir Dar University, P.O Box 26, Bahir Dar, Ethiopia
- d Technical University of Munich, TUM School of Life Sciences, Department of Life Science Engineering, Food Process Engineering, Weihenstephaner Berg 1, 85354, Freising Germany
- e Department of Petroleum Engineering, Knowledge University, Arbil, Iraq
- f Department of Mechanical Engineering of Biosystems, Faculty of Agriculture, University of Jiroft, Jiroft, Iran
- g Department of Biological and Agricultural Engineering, Faculty of Engineering Universiti Putra Malaysia, 43400, Serdang, Selangor, Malaysia
- h SMART Farming Technology Research Centre (SFTRC), Faculty of Engineering Universiti Putra Malaysia, 43400, Serdang, Selangor, Malaysia
- ⁱ Department of Food Sciences, Faculty of Science and Technology, Universiti Kebangsaan Malaysia, UKM, 43600, Bangi, Selangor Darul Ehsan, Malaysia
- ^j Innovation Center for Confectionary Technology (MANIS), Faculty of Science and Technology, Universiti Kebangsaan Malaysia, UKM, 43600, Bangi, Selangor Darul Ehsan, Malaysia
- k Department of Bioresource Engineering, Macdonald Campus, McGill University, 21,111 Lakeshore Road, Sainte-Anne-de-Bellevue, Montreal, Quebec, Canada, H9X 3V9
- ¹ Albrecht Daniel Thaer-Institute of Agricultural and Horticultural Sciences, Humboldt Universität zu Berlin, Berlin, Germany
- ^m Natural Resources Institute (NRI), Faculty of Engineering and Science, University of Greenwich, United Kingdom
- ⁿ WorldFish, Jalan Batu Maung, Batu Maung, 11900, Bayan Lepas, Penang, Malaysia
- ° Technische Universität Berlin, Institute of Food Biotechnology and Process Engineering, Berlin, Germany
- ^p Indian Council of Agricultural Research, New Delhi, India
- ^q Department of Agricultural and Biosystems Engineering, Kenyatta University, Nairobi, Kenya
- ^r Department of Energy Systems Engineering, Faculty of Agricultural Engineering, University of Agriculture, Faisalabad, Pakistan

ARTICLE INFO

Keywords: Digital Twins-based smart food drying Non-invasive measurements Dynamic optimization Mathematical models Advanced control

ABSTRACT

Digital Twins technology is rapidly growing and has the potential to revolutionize traditional food-processing methods. However, their application in food-drying processes is still in its infancy. This study aimed to explore how Digital Twins can be applied to food drying process. Traditionally, food drying is performed under constant conditions, where air temperature and velocity remain constant. However, the literature review shows that variable drying conditions (trajectories) can improve both energy efficiency and product quality. The challenge is that the trajectories are calculated based on what happened in the process, not what is currently happening. Digital Twins address this shortcoming by enabling decision making based on real-time data. In this conceptual review paper, physiochemical parameters as an element of the physical world of a Digital Twins-based smart food dryer is first presented. Next, potential sensors for building a digital counterpart of the physiochemical parameters are discussed. This is followed by mathematical models, dynamic optimization, and advanced control, which are the core elements of a decision-making and control unit. Finally, future research needs are discussed. This conceptual review paper will guide and give a solid insight to academic researchers, companies, and other potential stakeholders on merging Digital Twins and food drying technologies.

This article is part of a special issue entitled: Digital Twins published in Journal of Food Engineering.

^{*} Corresponding author.

^{**} Corresponding author. Leibniz Institute for Agricultural Engineering and Bioeconomy (ATB), Potsdam, Germany. E-mail addresses: aarefi@atb-potsdam.de (A. Arefi), Bsturm@atb-potsdam.de (B. Sturm).

1. Introduction

The high water content in fruits and vegetables provides a potential growing environment for microorganisms to accelerate spoilage. To mitigate microbial spoilage, drying technology has been of great interest, as water activity is reduced to hinder the growth of microorganisms. Dried fruits and vegetables are not only associated with a longer shelf life, but also lower expenses for transportation, storage, and packaging (Mousakhani-Ganjeh et al., 2021). Nevertheless, the drying process has been criticized for its negative impact on nutrients; dried apple slices, for instance, contain 70 % less vitamin C compared to fresh ones (Arefi et al., 2021) in convective drying. The advent of smart processing practices in the manufacturing industry in the context of the Industry 4.0 and 5.0 concepts promises to significantly advance the understanding of product-process interactions and the dynamics of changes of products in food processing (Sturm, 2018). In this context, the emerging concept of Digital Twins plays a crucial role. Digital Twins are defined as the virtual replica of real world (Verboven et al., 2020). In its first maturity stage, it was limited to simulating the physical entity, the so-called Digital Model. A digital model considers scenarios that could occur in the physical entity instead of the current state. To address this shortcoming, the digital model was further extended to a **Digital Shadow** by enabling real-time data transfer from the physical entity to the model. Nevertheless, the communication between physical and virtual entities was unidirectional. In other words, it was the physical world affecting the digital shadow, and not vice versa. Real-time optimization and control of a physical process is possible only if there exists bidirectional communication by which the digital shadow can send its feedback to the physical entity, which is called **Digital Twins**. Digital Twins resemble their physical counterparts in a way their appearance is not only similar but also show the same behavior, like a mirror (Kritzinger et al., 2018). Digital Twins consist of a physical entity, digital entity, and bidirectional communication between them. Indeed, in contrast to the traditional drying process, which usually relies on constant process conditions irrespective of the varations in raw material quality, Digital Twins-based smart food drying employs dynamic/variable drying conditions found to be superior to constant drying conditions (Jin et al., 2014b; Chen et al., 2020a; Olmos et al., 2002; Sturm, 2010; Sturm et al., 2009; Sujinda et al., 2021).

1.1. The-state-of-the-art of Digital Twins in food drying process

Digital Twins-based drying is still in its infancy, and in-depth research is needed to bring it to the real world. Martynenko (2017) highlighted the interdisciplinary nature of the research topic as a challenge postponing the development of intelligent dryers, as it requires knowledge of drying principles, Artificial Intelligence, computer vision, mathematical modeling, dynamic optimization, real-time control, and process automation. The earliest and unique effort given to the development of a Digital Twins-based dryer dates back to 2007, when Martynenko and Yang (2007) integrated a machine vision system into a pilot dryer to optimize both the drying time and quality index of ginseng roots. Their proposed system reduced the drying time from 240 to 90-110 h whilst meeting the quality criterion. Concurrently, Sturm and Hofacker (2007) proposed a system integrating a machine vision for a better understanding of the dynamic changes within the process based on the continuous monitoring of color changes. They found that product temperature-controlled drying has significant advantages over air temperature control in terms of the reduction of color changes, drying time, and thermal stress of the product. Based on the continuous measurement of color changes, they determined the inflection points in the degree of change in ΔE at the phase transition. This information was used in a follow-up study to change processing conditions in a stepwise manner (Sturm and Hofacker, 2010).

Most of existing studies have focused on individual components of a Digital Twins-based smart food drying rather than developing a fully

integrated system. Prawiranto et al., (2021) developed a digital model for solar drying, combining a mechanistic drying model with fruit quality degradation models to assess the impact of weather variations on drying time and final product quality. The model effectively demonstrated differences in drying outcomes across various drying runs. They further proposed integrating real-time or forecasted weather data into the model to enable real-time control of solar dryers. A recent study by Schemminger et al. (2024) developed a physics-based model enhanced with Monte Carlo simulations to capture the natural variability in fresh carrot slices and during convective drying. The model provided non-invasive insights into hygrothermal dynamics and β -carotene degradation. To reduce the computational burden of mechanistic drying models, Ghosh and Datta (2023) developed a deep learning-based surrogate model by training on simulation data from a multiphysics drying model. This approach maintained high spatial and temporal resolution while significantly improving computational efficiency. A dynamic optimization approach was applied to enhance both energy efficiency and vitamin C retention during the drying of broccoli (Jin et al., 2014b). By modeling the kinetics of moisture loss and nutrient degradation, optimal trajectories for air temperature and flow rate were identified. The optimized strategy, featuring a descending-ascending temperature profile and a gradually reduced airflow, achieved significantly higher energy efficiency (65 %) and vitamin C retention (55 %) compared to conventional static drying (28 % and 32 %, respectively). Sabat et al. (2022) integrated a computer vision system into a dryer for inline monitoring of potato slice color changes during drying. The extracted chromatic features served as input to a Long Short-Term Memory (LSTM) model, which accurately predicted the corresponding moisture content, demonstrating the effectiveness of combining vision-based sensing with deep learning for non-destructive moisture estimation. Advanced non-invasive sensors, such as near- and mid-infrared hyperspectral imaging (Su et al., 2020) and low-field nuclear magnetic resonance (Sun et al., 2021c), have shown promising results for monitoring moisture content changes during drying.

With the rapid advancement of Artificial Intelligence, non-invasive sensors, and computing powers, the emergence of digital twin-based approaches in food drying processes is increasingly anticipated. However, there remains ambiguity regarding the integration of Digital Twins into food drying systems. This paper seeks to clarify this gap by presenting a structured framework for implementing Digital Twins in food drying applications. It offers a step-by-step guide to assist researchers and practitioners in developing a smart dryer powered by digital twin technology.

1.2. How to integrate Digital Twins components to develop a smart food drying process

Fig. 1 shows a schematic representation of Digital Twins-based smart food drying process. The Physical entity (red dashed rectangle) consists of the environment where the drying process is carried out (chamber, tunnel, etc.); the product to be dried; and the sensors (see Section 3) used to measure the relevant process/product variables (Section 2). If the available sensors are able to measure the relevant process variables, then such measurements can be fed directly to the Virtual entity (see Section 4.1). If this is not the case (for example when only temperature measurements are available), a software sensor (Lara-Cisneros and Dochain, 2018), that combines mathematical models and hardware sensor measurements, can be used to estimate unmeasured process/product variables, which are fed to the Virtual entity. A dynamic optimization procedure (Section 4.2.1) can be used to compute the optimal trajectories or set points of the variables to be controlled in the process (Section 2). Once such reference trajectories are computed, they are sent to a controller (Section 4.2.2) to compute the values of the variables that can be manipulated in the process (input variables/controls) such as air velocity, chamber temperature, etc. The output of the controller is sent to the process so that the reference trajectories/set points are met. To

minimize the impact of modeling errors, the above-mentioned procedure can be performed recursively. In this regard, when new process measurements are available, they are fed to the Virtual entity to recompute the reference trajectories. Besides, such measurements can be also used to update the model parameters and improve its predictive capabilities by fitting the model predictions to the experimental data. The Digital Twins can integrate other modules to identify hardware malfunctions (Fault detection (Massei et al., 2025)); to ensure consistency among the sensor measurements (Data reconciliation (Pitarch et al., 2019)); to estimate states (Kalman filter or Moving horizon Estimation (Allgöwer et al., 1999)); or to estimate and account for process product variability (Oliveira-Silva et al., 2021), among other.

1.3. Challenges of Digital Twins-based smart food drying systems

The number of parameters transferred between physical and virtual entities and their accuracy, the so-called fidelity, is foreseen as a challenge. Fruits and vegetables are complex matrices containing a number of micronutrients. However, the low concentration of micronutrients, given the high amount of water, raises concerns about their accurate prediction. A digital replica of the full spectrum of micronutrients, if not impossible, requires a number of sensors. As a result, the initial cost of a digital twin-based drying process can be high. Moreover, the development of robust predictive models requires a reasonable number of tedious and costly quality measurements. Furthermore, the high-tech level of the Digital twins-based smart food drying process brings about special maintenance and operator training. The data storage cost is another issue. Another challenge is the expandability of a Digital Twinsbased dryer for a broad spectrum of fruits and vegetables. Nevertheless, Digital-Twins is seen as the future of food processing systems, and the above-mentioned challenges need to be addressed.

2. Physicochemical parameters

During the drying of fruits and vegetables, a range of quality attributes, such as water activity, color, texture, rehydration capacity, shrinkage, total phenolic content, pigments (e.g., anthocyanins, chlorophyll, and carotenoids), vitamin C, and aroma, undergo significant changes. These attributes are not only critical for consumer acceptance but also reflect the nutritional and functional value of the final product. Their retention or degradation depends heavily on the drying method and conditions, including temperature, air velocity, and humidity. Understanding how these attributes respond to different drying conditions is essential for optimizing the process and ensuring product quality. Table 1 summarizes findings from the literature on how these attributes are impacted across various drying studies. As presented in Table 1, the quality attributes show different behaviors which can be mathematically modeled as presented in section 4.1. However, such models are often limited in their generalizability, as their accuracy depends on factors such as drying conditions, raw material properties, and processing parameters. To address this shortcoming, it is essential to continuously update these models using real-time sensor data. To this end, potential sensors for real-time monitoring are presented in the following section.

3. Potential sensors for Digital Twins-based food drying system

Overall, a fusion of sensors is expected to result in a reliable and comprehensive digital representation of quality attributes. Nevertheless, the following points are worth considering.

 Imaging techniques are preferred over point-based techniques because they deliver spatial information and their field of view is larger, by which several samples can be simultaneously monitored. Furthermore, shrinkage/bending causes changes in the distance and/ or angle between the point-based optical probes and samples, which can influence the received light. However, point-based techniques

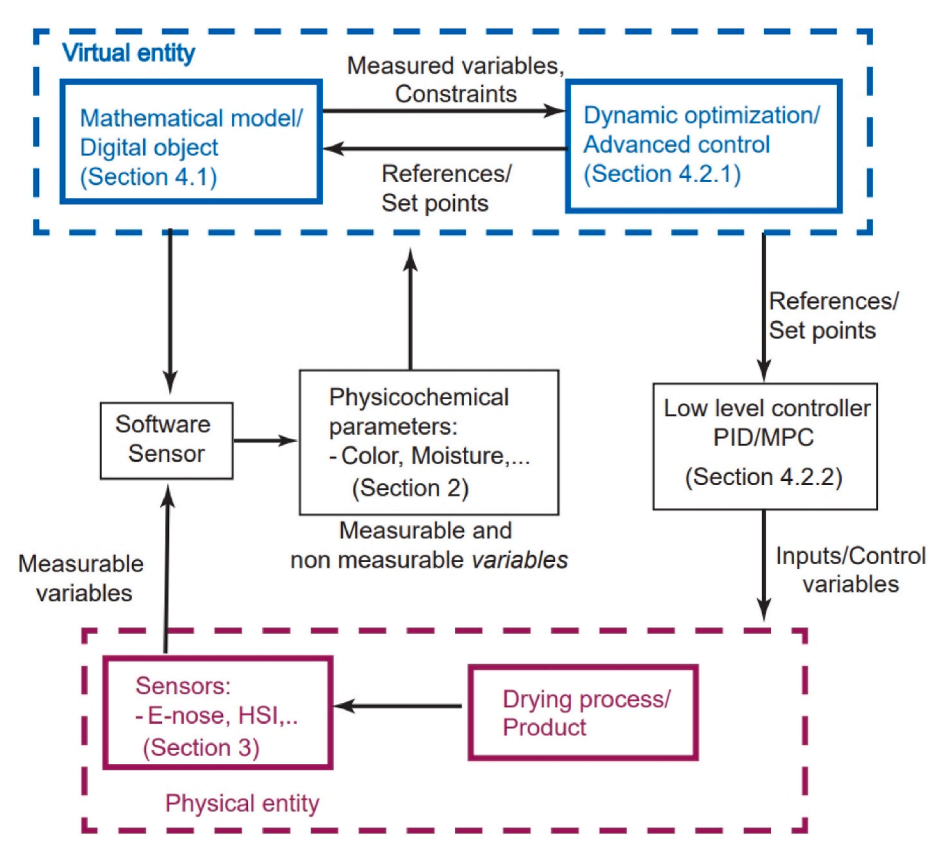


Fig. 1. The concept of Digital Twins-based smart food drying process.

 Table 1

 The impact of drying parameters on quality attributes of fruits and vegetables.

Physicochemical attributes	Description	Findings	Reference	Physicocl attributes
Water activity	Air temperature: 40, 50, and 60 °C Final dried condition: moiture content (MC) of 10 % w.b	Water activity of beetroot pulp dried at high temperatures was low.	Preethi et al. (2020)	
	Air temperature: 313.15–373.15 K Final dried condition: constant final weight	Water activity of dried guabiju pulp was low with high drying temperature.	Bombana et al. (2023)	Texture
	Air temperature: 40, 50, and 60 °C Drying time: 24, 30, and 36 h Final dried condition: unspecified	The drying conditions with higher temperatures (60 °C and 70 °C) and longer times (30 h and 36 h) resulted in lower water activity in onion.	Sarkar et al. (2023)	
	Air temperature: 40, 50, 60, 70, and 80 °C Air velocity: 1.0 and 1.5 m/s Final dried condition: constant final weight	Higher temperatures correlated with lower water activity in dried red-fleshed dragon. Air velocity did not have a significant effect on water activity.	Mahayothee et al. (2019)	
	Air temperature: 45, 55, and 65 °C Sample thicknesses: 1.5 and 5 mm Air velocity: 0.2 m/s Final dried condition: unspecified	Higher air temperature and air velocity settings correlated with lower water activity in dried apple chips. Thicker samples exhibited higher water activity.	Demiray et al. (2023)	
	Air temperature: 50, 60, and 70 °C Air velocity: 0.5 and 1 m/s Final dried condition: constant final weight	Higher temperature and air velocity settings parameters settings correlated with lower water activity in dried feijoa fruit.	Castro et al. (2023)	
	Air temperature: 40, 50, 60, and 70 °C Air velocity: 0.5, 1, and 2 m/s Final dried condition: constant final weight	Higher air velocity correlated with lower water activity in dried lemongrass leaves. Air temperature did not significantly (p > 0.05) influence the water activity in the dried leaves.	Mujaffar and John (2018)	Rehydrat
Color	Air temperature: 60, 70, and 80 °C	As the air temperature increased, the color changes of kiwi slices increased	Tepe et al. (2022)	
	Air temperature: 50, 60, and 70 °C	Color changes of yam slices increased as the temperature increased.	Sahoo et al. (2022)	
	Air temperature: 50, 60, and 70 $^{\circ}\text{C}$	Pomegranate color changes increased	Kaveh et al. (2021)	

Table 1 (continued)

Physicochemical attributes	Description	Findings	Reference
		with an increase in	
		the temperature.	
	Air temperature:	The color changes	Tan et al. (2022)
	40, 55, and 70 °C	in blood-flesh	
		peach were	
		negatively	
		correlated with temperature.	
Texture	Air temperature:	Temperature.	Di Scala et al.
Texture	50, 60, 70, 80,	exposure reduced	(2011)
	and 90 °C	firmness of pepino	
		fruit (Solanum after	
		convective drying.	
	Air temperature:	Fracturability and	Kian-Pour and
	110, 115, and	crispness were	Karatas (2019)
	120 °C	shown to be higher	
		while hardness was slower at higher	
		temperatures in	
		convectively dried	
		apple slices.	
	Air temperature:	The firmness of	Antal et al. (2015
	75 °C	apple cubes	
		convectively dried	
		at 75 °C was higher	
		than in fresh cubes.	
	Air temperature:	Hardness,	Quispe-Fuentes
	40, 50, 60, 70, and 80 °C	cohesiveness, chewiness, and	et al. (2017)
	and 80 °C	resilience were	
		lower while	
		springiness and	
		adhesiveness were	
		higher in	
		convectively dried	
		maqui berry than in	
		fresh samples at all	
		temperature	
		settings.	
		Springiness,	
		cohesiveness, and gumminess of the	
		samples at 80 °C	
		were notably	
		similar to fresh	
		samples.	
	Air temperature:	Hot-air drying	Alonzo-Macías
	50 °C	increased the	Alonzo-Macías et al. (2014)
	50 °C Slice thickness:	increased the hardness and	
	50 °C Slice thickness: 4–5 mm	increased the hardness and brittleness in	
	50 °C Slice thickness: 4–5 mm Air velocity: 1.2	increased the hardness and brittleness in strawberry fruit	
	50 °C Slice thickness: 4–5 mm Air velocity: 1.2 m/s	increased the hardness and brittleness in strawberry fruit and in turn the	
	50 °C Slice thickness: 4–5 mm Air velocity: 1.2 m/s Final dried	increased the hardness and brittleness in strawberry fruit and in turn the crunchiness and	
	50 °C Slice thickness: 4–5 mm Air velocity: 1.2 m/s	increased the hardness and brittleness in strawberry fruit and in turn the crunchiness and crispiness in the	
Rehydration	50 °C Slice thickness: 4–5 mm Air velocity: 1.2 m/s Final dried condition: MC 3	increased the hardness and brittleness in strawberry fruit and in turn the crunchiness and	
Rehydration	50 °C Slice thickness: 4–5 mm Air velocity: 1.2 m/s Final dried condition: MC 3 % d.b.	increased the hardness and brittleness in strawberry fruit and in turn the crunchiness and crispiness in the dried slices.	et al. (2014)
Rehydration	50 °C Slice thickness: 4-5 mm Air velocity: 1.2 m/s Final dried condition: MC 3 % d.b. Air temperature	increased the hardness and brittleness in strawberry fruit and in turn the crunchiness and crispiness in the dried slices. Rehydration ratio	et al. (2014) Aradwad et al.
Rehydration	50 °C Slice thickness: 4-5 mm Air velocity: 1.2 m/s Final dried condition: MC 3 % d.b. Air temperature	increased the hardness and brittleness in strawberry fruit and in turn the crunchiness and crispiness in the dried slices. Rehydration ratio of apple slices increased with increasing	et al. (2014) Aradwad et al.
Rehydration	50 °C Slice thickness: 4–5 mm Air velocity: 1.2 m/s Final dried condition: MC 3 % d.b. Air temperature 60, 65, and 75 °C	increased the hardness and brittleness in strawberry fruit and in turn the crunchiness and crispiness in the dried slices. Rehydration ratio of apple slices increased with increasing temperature.	et al. (2014) Aradwad et al. (2023)
Rehydration	50 °C Slice thickness: 4–5 mm Air velocity: 1.2 m/s Final dried condition: MC 3 % d.b. Air temperature 60, 65, and 75 °C	increased the hardness and brittleness in strawberry fruit and in turn the crunchiness and crispiness in the dried slices. Rehydration ratio of apple slices increased with increasing temperature. Wormwood leaves	et al. (2014) Aradwad et al.
Rehydration	50 °C Slice thickness: 4–5 mm Air velocity: 1.2 m/s Final dried condition: MC 3 % d.b. Air temperature 60, 65, and 75 °C	increased the hardness and brittleness in strawberry fruit and in turn the crunchiness and crispiness in the dried slices. Rehydration ratio of apple slices increased with increasing temperature. Wormwood leaves dried at higher air	et al. (2014) Aradwad et al. (2023)
Rehydration	50 °C Slice thickness: 4–5 mm Air velocity: 1.2 m/s Final dried condition: MC 3 % d.b. Air temperature 60, 65, and 75 °C	increased the hardness and brittleness in strawberry fruit and in turn the crunchiness and crispiness in the dried slices. Rehydration ratio of apple slices increased with increasing temperature. Wormwood leaves dried at higher air temperature	et al. (2014) Aradwad et al. (2023)
Rehydration	50 °C Slice thickness: 4–5 mm Air velocity: 1.2 m/s Final dried condition: MC 3 % d.b. Air temperature 60, 65, and 75 °C	increased the hardness and brittleness in strawberry fruit and in turn the crunchiness and crispiness in the dried slices. Rehydration ratio of apple slices increased with increasing temperature. Wormwood leaves dried at higher air temperature exhibited higher	et al. (2014) Aradwad et al. (2023)
Rehydration	50 °C Slice thickness: 4–5 mm Air velocity: 1.2 m/s Final dried condition: MC 3 % d.b. Air temperature 60, 65, and 75 °C Air temperature: 50, 60, and 70 °C	increased the hardness and brittleness in strawberry fruit and in turn the crunchiness and crispiness in the dried slices. Rehydration ratio of apple slices increased with increasing temperature. Wormwood leaves dried at higher air temperature exhibited higher rehydration ratio.	et al. (2014) Aradwad et al. (2023) Beigi (2017)
Rehydration	50 °C Slice thickness: 4–5 mm Air velocity: 1.2 m/s Final dried condition: MC 3 % d.b. Air temperature 60, 65, and 75 °C Air temperature: 50, 60, and 70 °C	increased the hardness and brittleness in strawberry fruit and in turn the crunchiness and crispiness in the dried slices. Rehydration ratio of apple slices increased with increasing temperature. Wormwood leaves dried at higher air temperature exhibited higher rehydration ratio. Hawthorn samples	et al. (2014) Aradwad et al. (2023) Beigi (2017) Aral and Beşe
Rehydration	50 °C Slice thickness: 4–5 mm Air velocity: 1.2 m/s Final dried condition: MC 3 % d.b. Air temperature 60, 65, and 75 °C Air temperature: 50, 60, and 70 °C	increased the hardness and brittleness in strawberry fruit and in turn the crunchiness and crispiness in the dried slices. Rehydration ratio of apple slices increased with increasing temperature. Wormwood leaves dried at higher air temperature exhibited higher rehydration ratio. Hawthorn samples dried at higher air	et al. (2014) Aradwad et al. (2023) Beigi (2017)
Rehydration	50 °C Slice thickness: 4–5 mm Air velocity: 1.2 m/s Final dried condition: MC 3 % d.b. Air temperature 60, 65, and 75 °C Air temperature: 50, 60, and 70 °C	increased the hardness and brittleness in strawberry fruit and in turn the crunchiness and crispiness in the dried slices. Rehydration ratio of apple slices increased with increasing temperature. Wormwood leaves dried at higher air temperature exhibited higher rehydration ratio. Hawthorn samples dried at higher air temperature air temperature.	et al. (2014) Aradwad et al. (2023) Beigi (2017) Aral and Beşe
Rehydration	50 °C Slice thickness: 4–5 mm Air velocity: 1.2 m/s Final dried condition: MC 3 % d.b. Air temperature 60, 65, and 75 °C Air temperature: 50, 60, and 70 °C	increased the hardness and brittleness in strawberry fruit and in turn the crunchiness and crispiness in the dried slices. Rehydration ratio of apple slices increased with increasing temperature. Wormwood leaves dried at higher air temperature exhibited higher rehydration ratio. Hawthorn samples dried at higher air	et al. (2014) Aradwad et al. (2023) Beigi (2017) Aral and Beşe
Rehydration	50 °C Slice thickness: 4–5 mm Air velocity: 1.2 m/s Final dried condition: MC 3 % d.b. Air temperature 60, 65, and 75 °C Air temperature: 50, 60, and 70 °C	increased the hardness and brittleness in strawberry fruit and in turn the crunchiness and crispiness in the dried slices. Rehydration ratio of apple slices increased with increasing temperature. Wormwood leaves dried at higher air temperature exhibited higher rehydration ratio. Hawthorn samples dried at higher air temperature showed higher	et al. (2014) Aradwad et al. (2023) Beigi (2017) Aral and Beşe
Rehydration	50 °C Slice thickness: 4–5 mm Air velocity: 1.2 m/s Final dried condition: MC 3 % d.b. Air temperature 60, 65, and 75 °C Air temperature: 50, 60, and 70 °C	increased the hardness and brittleness in strawberry fruit and in turn the crunchiness and crispiness in the dried slices. Rehydration ratio of apple slices increased with increasing temperature. Wormwood leaves dried at higher air temperature exhibited higher rehydration ratio. Hawthorn samples dried at higher air temperature showed higher rehydration ratio.	et al. (2014) Aradwad et al. (2023) Beigi (2017) Aral and Beşe (2016)
Rehydration	50 °C Slice thickness: 4–5 mm Air velocity: 1.2 m/s Final dried condition: MC 3 % d.b. Air temperature 60, 65, and 75 °C Air temperature: 50, 60, and 70 °C Air temperature: 50, 60, and 70 °C	increased the hardness and brittleness in strawberry fruit and in turn the crunchiness and crispiness in the dried slices. Rehydration ratio of apple slices increased with increasing temperature. Wormwood leaves dried at higher air temperature exhibited higher rehydration ratio. Hawthorn samples dried at higher air temperature showed higher rehydration ratio. The lowest	et al. (2014) Aradwad et al. (2023) Beigi (2017) Aral and Beşe (2016)

Table 1 (continued)

Table 1 (continued)

Physicochemical attributes	Description	Findings	Reference	Physicochemical attributes	Description	Findings	Reference
	Air temperature: 45, 50, 55, and 60 °C	The higher temperature, the higher rehydration	Xu et al. (2022)		0.5, 0.9, and 1.3 m/s.	decreasing drying temperature and air velocity.	
		ratio mushroom had.		Total phenolic content	Air temperature: 50, 60, and 70 °C	The total phenolic content of pumpkin	Chikpah et al. (2022)
	Air temperature: 45, 55, 65, and 75 °C	As the temperature increased, the rehydration ratio of	Izli and Polat (2019)			increased as the temperature increased.	
	Air temperature: 60, 65, 70, and 75 °C	quince decreased. With the increase of temperature, rehydration ratio of Phyllanthus emblica decreased.	Huang et al. (2023)		Air temperature: 60, 70, and 80 °C	Kiwi slices dried at high temperature were associated with a higher concentration of total phenolic	(Izli et al., 2017; Tepe et al., 2022)
	Air temperature: of 50, 60, and 70 °C.	Mint leaves dried at higher air temperature exhibited lower rehydration ratio.	Beigi (2017)		Air temperature: 40, 50, and 60 $^{\circ}$ C	content. The increase in drying temperature increased total phenolic content of	Kheto et al. (2021)
	Air temperature: 50, 60, and 70 °C Air velocity: 0.5, 1, and 1.5 m/s Slice thickness: 3,	The highest rehydration ratio of yam slices was associated with the highest air velocity.	Ojediran et al. (2020)		Air temperature: 40, 50, and 60 $^{\circ}$ C	paprika. As the temperature increased, total phenolic content of beetroots	Preethi et al. (2020)
	6, and 9 mm Air temperature: 50, 60, and 70 °C Air velocity: 5, 7, and 9 m/s	With the increase of air velocity, the rehydration ratio of quince slices	Goli et al. (2023)		Air temperature: 60 and 80 °C	decreased. Increasing air temperature decreased total phenolic content of	Kamble et al. (2022)
ehydration	Air temperature: 60 and 80 °C Air velocity: 0.2 and 0.7 m/s	increased. An increase in the temperature and air velocity caused a decrease in rehydration ratio of chicory roots.	Balzarini et al. (2018)		Air temperature: 20, 40, and 70 $^{\circ}\text{C}$	green banana. High temperature lead to high degradation of phenolic contents compared to low temperature drying	Joshi et al. (2011)
	Air temperature: 40, 60, and 75 °C Air velocity: 0.6 m/s Material thickness:4, 7,	Air temperature did not influence the rehydration ratio of purple-speckled cocoyam	Ndisya et al. (2020)		Air temperature: 60–70 °C	and freeze drying. Hot air drying at 60–70 °C resulted in approximately 40 % decrease in both total	Guiné et al. (2015)
hrinkage	and 10 mm Air temperature: 55, 65, and 75 °C	Pomegranate shrinkage increased with increasing drying temperature	Sufer and Palazoglu (2019)		Air temperature: 55–75 °C	phenolics and antioxidant activity. Increasing drying temperature up to 75 °C resulted in	Da Cruz et al. (2012)
	Air temperature: 50, 60, 70 and 80 °C	As the temperature increased, the potato shrinkage increased	Thuy et al. (2022)			higher levels of phenolic compounds and lycopene in the	
	Air temperatures 50, 60, and 70 °C Air temperatures	Shrinkage of papaya increased as temperature increased Shrinkage of melon	Islam et al. (2019) Darvishi et al.	Total phenolic content	Air temperature: 55–75 °C	dried tomatoes. Increasing drying temperature up to 75 °C resulted in higher levels of	Da Cruz et al. (2012)
	of 40, 50, 60, and 70 °C	slices decreased as the temperature increased.	(2015)			phenolic compounds and lycopene in the	
	Air temperatures: 50, 60, and 70 °C.	Shrinkage of plum increased with decreasing drying temperature	Ojediran et al. (2021)		Air temperature: 50–90 °C	dried tomatoes. Higher the drying temperature resulting in lower	López et al. (2010)
	Air temperatures: 50, 60, 70, and 80 °C Air velocity: 0.5,	An increase in temperature caused an increase in pear slices shrinkage,	Kalantari et al. (2023)		Air temperature:	the value of phenolic components. The higher air	Del Razola-Díaz
	1, and 1.5 m/s	but the air velocity did not have a significant effect on shrinkage.			40, 60, and 80 °C Air velocity: 0, 0.8, and 1.6 m/s	velocity, the highest concentration of total phenolic	et al. (2023)
	Air temperatures 50, 60, and 70 °C Air velocities of	Shrinkage of hawthorn fruit increased with	Aral and Beşe (2016)		Air temperature: 50, 60, and 70 °C	content in orange. Total phenolic content of paprika	Sasikumar et al. (2023) ntinued on next page

Table 1 (continued)

Table 1 (continued)

Physicochemical attributes	Description	Findings	Reference	Physicochemical attributes	Description	Findings	Reference
	Air velocity: 1.5,	was higher when				happened when	
	2, and 2.5 m/s	drying was				drying temperature	
		conducted at				increased from 50	
		higher air velocity.	B 1 1 1 1	D' .		to 80 °C.	***
	Air temperature:	Lowering the air	Rajendran et al.	Pigments	Air temperature:	Purple sweet potato	Wang et al.
	50, 60, 70, and 80 °C	temperature and velocity resulted	(2023)		60–110 °C	dried at 110 °C contained the	(2020)
	Air velocity: 0.8,	higher loss of total				lowest	
	2.1, and 3.4 m/s	phenolic content in				concentration of	
	211, and 511 111/5	Turkey berry.				anthocyanin.	
	Air temperature:	Total phenolic	Sarpong et al.		Air temperature:	Raspberries dried	Stamenković
	60, 70, and 80 $^{\circ}\text{C}$	content of	(2021)		60, 70, and 80 $^{\circ}\text{C}$	at 70 $^{\circ}\text{C}$ had the	et al. (2019)
	Relative	pineapple slices				highest retention	
	humidity: 10, 20,	was higher when				(56 %) of	
	and 30 %	drying was				anthocyanin.	*** 1 *
		conducted at			Air temperature:	Strawberries dried	Méndez-Lagunas
		higher relative humidity.			50 and 60 °C	at 50 and 60 °C showed 26 % and	et al. (2017)
	Air temperature:	Higher relative	Matys et al.			45 % loss of	
	55, 70, and 85 °C	humidity was	(2023)			anthocyanins.	
	Relative	related to a higher	(====)		Air temperature:	Anthocyanin loss	Rodríguez et al.
	humidity: 1.5 and	total phenolic			40 and 80 °C	increased from 48	(2016)
	10 g/m3	content in apple				to 60 % as the	
		slices.				temperature	
Pigments	Air temperature:	The higher	Lu et al. (2015)			elevated.	
	55–95 °C	temperature, the			Air temperature:	Blueberries dried at	Zia and Alibas
		lower retention of			50, 70, and 90 °C	90 °C showed a	(2021)
		chlorophyll in mint				higher retention of	
	Air temperature:	leaves. The highest loss of	Beigi (2019)	Vitamin C	Air temperature:	anthocyanins Increasing the	Kaya et al. (2010
	40, 50, and 60 °C	chlorophyll (36 %)	Deigi (2019)	vitalilli C	25, 35, 45, 55,	drying air	Raya et al. (2010
	10, 50, and 60 G	in mint leaves was			and 65 °C	temperature	
		related to the air			Relative	accelerates the	
		temperature of			humidity: 40, 55,	degradation of	
		60 °C.			70, and 85	vitamin C in dried	
	Air temperature:	Chlorophyll	Kheto et al.		Air velocity: 0.3,	kiwi fruits, while	
	40–60 °C	content of green	(2021)		0.6, and 0.9 m/s	higher relative	
		paprika decreased				humidity of the	
		from 27.17 to				drying air reduces	
		16.88 μg/g dry matter when			Air temperature:	this degradation. The retention of	Ek et al. (2018)
		temperature			40, 55, and 70 °C	vitamin decreased	ER et al. (2016)
		increased.			Relative	from 72.8 to 12.5 %	
	Air temperature:	Chlorophyll	Mokhtar and		humidity: 38,	with increasing	
	50–70 °C	retention in Jew's	Morsy (2014)		24.4, and 16.1	temperature	
		mallow leaves			Air temperature:	The retention of	Sehrawat et al.
		increased as the air			60, 70, and 80 °C		
					60, 70, and 80 °C	vitamin C in mango	(2018)
		temperature			60, 70, and 80 °C	during hot air	(2018)
		temperature increased.	5		60, 70, and 80 °C	during hot air drying was higher	(2018)
	Air temperature:	temperature increased. The higher	Demiray et al.		60, 70, and 80 °C	during hot air drying was higher at 60 °C, while the	(2018)
	Air temperature: 50–100 °C	temperature increased. The higher temperature, the	Demiray et al. (2013)		60, 70, and 80 °C	during hot air drying was higher at 60 °C, while the differences in	(2018)
	•	temperature increased. The higher temperature, the higher loss of	•		60, 70, and 80 °C	during hot air drying was higher at 60 °C, while the differences in retention were not	(2018)
	•	temperature increased. The higher temperature, the	•		60, 70, and 80 °C	during hot air drying was higher at 60 °C, while the differences in retention were not significant between	(2018)
	50–100 °C	temperature increased. The higher temperature, the higher loss of lycopene and beta- carotene.	(2013)		Air temperature:	during hot air drying was higher at 60 °C, while the differences in retention were not	
	•	temperature increased. The higher temperature, the higher loss of lycopene and beta-	•			during hot air drying was higher at 60 °C, while the differences in retention were not significant between 70 °C and 80 °C.	
	50–100 °C Air temperature:	temperature increased. The higher temperature, the higher loss of lycopene and beta- carotene. Alpha- and beta-	(2013) Ouyang et al.		Air temperature:	during hot air drying was higher at 60 °C, while the differences in retention were not significant between 70 °C and 80 °C. Vitamin C of	
	50–100 °C Air temperature:	temperature increased. The higher temperature, the higher loss of lycopene and beta- carotene. Alpha- and beta- carotenes in	(2013) Ouyang et al.		Air temperature: 60, 65, 70, and	during hot air drying was higher at 60 °C, while the differences in retention were not significant between 70 °C and 80 °C. Vitamin C of broccoli florets	
	50–100 °C Air temperature:	temperature increased. The higher temperature, the higher loss of lycopene and betacarotene. Alpha- and betacarotenes in pumpkin slices were found more thermostable than	(2013) Ouyang et al.		Air temperature: 60, 65, 70, and 75 °C Air velocity: 9 m/ s	during hot air drying was higher at 60 °C, while the differences in retention were not significant between 70 °C and 80 °C. Vitamin C of broccoli florets decreases rapidly as the drying temperature	
	50–100 °C Air temperature:	temperature increased. The higher temperature, the higher loss of lycopene and beta- carotene. Alpha- and beta- carotenes in pumpkin slices were found more thermostable than dihydroxy	(2013) Ouyang et al.		Air temperature: 60, 65, 70, and 75 °C Air velocity: 9 m/ s Blanching: 90 s	during hot air drying was higher at 60 °C, while the differences in retention were not significant between 70 °C and 80 °C. Vitamin C of broccoli florets decreases rapidly as the drying temperature increases	Liu et al. (2019b
	50–100 °C Air temperature: 60–100 °C	temperature increased. The higher temperature, the higher loss of lycopene and betacarotene. Alpha- and betacarotenes in pumpkin slices were found more thermostable than dihydroxy xanthophylls.	(2013) Ouyang et al. (2022)		Air temperature: 60, 65, 70, and 75 °C Air velocity: 9 m/ s Blanching: 90 s Air temperature:	during hot air drying was higher at 60 °C, while the differences in retention were not significant between 70 °C and 80 °C. Vitamin C of broccoli florets decreases rapidly as the drying temperature increases Vitamin C content	Liu et al. (2019b
	50–100 °C Air temperature: 60–100 °C	temperature increased. The higher less of lycopene and betacarotene. Alpha- and betacarotenes in pumpkin slices were found more thermostable than dihydroxy xanthophylls. Losses over 50 %	Ouyang et al. (2022) Piyarach et al.		Air temperature: 60, 65, 70, and 75 °C Air velocity: 9 m/ s Blanching: 90 s Air temperature: 40, 50, and 60 °C	during hot air drying was higher at 60 °C, while the differences in retention were not significant between 70 °C and 80 °C. Vitamin C of broccoli florets decreases rapidly as the drying temperature increases Vitamin C content of tomato and	Liu et al. (2019b
	50–100 °C Air temperature: 60–100 °C	temperature increased. The higher temperature, the higher loss of lycopene and betacarotene. Alpha- and betacarotenes in pumpkin slices were found more thermostable than dihydroxy xanthophylls. Losses over 50 % happened in alpha-	(2013) Ouyang et al. (2022)		Air temperature: 60, 65, 70, and 75 °C Air velocity: 9 m/s Blanching: 90 s Air temperature: 40, 50, and 60 °C Air velocity: 1.5	during hot air drying was higher at 60 °C, while the differences in retention were not significant between 70 °C and 80 °C. Vitamin C of broccoli florets decreases rapidly as the drying temperature increases Vitamin C content of tomato and sweet pepper	Liu et al. (2019b
	50–100 °C Air temperature: 60–100 °C	temperature increased. The higher temperature, the higher loss of lycopene and beta-carotene. Alpha- and beta-carotenes in pumpkin slices were found more thermostable than dihydroxy xanthophylls. Losses over 50 % happened in alpha-carotene, beta-	Ouyang et al. (2022) Piyarach et al.		Air temperature: 60, 65, 70, and 75 °C Air velocity: 9 m/ s Blanching: 90 s Air temperature: 40, 50, and 60 °C	during hot air drying was higher at 60 °C, while the differences in retention were not significant between 70 °C and 80 °C. Vitamin C of broccoli florets decreases rapidly as the drying temperature increases Vitamin C content of tomato and sweet pepper decreased with	Liu et al. (2019b
	50–100 °C Air temperature: 60–100 °C	temperature increased. The higher temperature, the higher loss of lycopene and betacarotene. Alpha- and betacarotenes in pumpkin slices were found more thermostable than dihydroxy xanthophylls. Losses over 50 % happened in alphacarotene, betacarotene, and	Ouyang et al. (2022) Piyarach et al.		Air temperature: 60, 65, 70, and 75 °C Air velocity: 9 m/s Blanching: 90 s Air temperature: 40, 50, and 60 °C Air velocity: 1.5	during hot air drying was higher at 60 °C, while the differences in retention were not significant between 70 °C and 80 °C. Vitamin C of broccoli florets decreases rapidly as the drying temperature increases Vitamin C content of tomato and sweet pepper decreased with increasing	Liu et al. (2019b
	50–100 °C Air temperature: 60–100 °C	temperature increased. The higher temperature, the higher loss of lycopene and beta-carotene. Alpha- and beta-carotenes in pumpkin slices were found more thermostable than dihydroxy xanthophylls. Losses over 50 % happened in alpha-carotene, beta-	Ouyang et al. (2022) Piyarach et al.		Air temperature: 60, 65, 70, and 75 °C Air velocity: 9 m/s Blanching: 90 s Air temperature: 40, 50, and 60 °C Air velocity: 1.5	during hot air drying was higher at 60 °C, while the differences in retention were not significant between 70 °C and 80 °C. Vitamin C of broccoli florets decreases rapidly as the drying temperature increases Vitamin C content of tomato and sweet pepper decreased with	Liu et al. (2019b
	50–100 °C Air temperature: 60–100 °C Air temperature: 65 °C	temperature increased. The higher temperature, the higher loss of lycopene and betacarotene. Alpha- and betacarotenes in pumpkin slices were found more thermostable than dihydroxy xanthophylls. Losses over 50 % happened in alphacarotene, betacarotene, and lutein of pumpkin.	Ouyang et al. (2022) Piyarach et al. (2020)		Air temperature: 60, 65, 70, and 75 °C Air velocity: 9 m/s Blanching: 90 s Air temperature: 40, 50, and 60 °C Air velocity: 1.5 m/s	during hot air drying was higher at 60 °C, while the differences in retention were not significant between 70 °C and 80 °C. Vitamin C of broccoli florets decreases rapidly as the drying temperature increases Vitamin C content of tomato and sweet pepper decreased with increasing temperature.	Liu et al. (2019b Kaur et al. (2020
	50–100 °C Air temperature: 60–100 °C Air temperature: 65 °C	temperature increased. The higher temperature, the higher loss of lycopene and betacarotene. Alpha- and betacarotenes in pumpkin slices were found more thermostable than dihydroxy xanthophylls. Losses over 50 % happened in alphacarotene, betacarotene, and lutein of pumpkin. Apricot fruit dried	Ouyang et al. (2022) Piyarach et al. (2020) Albanese et al.		Air temperature: 60, 65, 70, and 75 °C Air velocity: 9 m/s Blanching: 90 s Air temperature: 40, 50, and 60 °C Air velocity: 1.5 m/s Air temperature:	during hot air drying was higher at 60 °C, while the differences in retention were not significant between 70 °C and 80 °C. Vitamin C of broccoli florets decreases rapidly as the drying temperature increases Vitamin C content of tomato and sweet pepper decreased with increasing temperature. Degradation of	Liu et al. (2019b Kaur et al. (2020 Kumar et al.
	50–100 °C Air temperature: 60–100 °C Air temperature: 65 °C	temperature increased. The higher less of lycopene and betacarotene. Alpha- and betacarotenes in pumpkin slices were found more thermostable than dihydroxy xanthophylls. Losses over 50 % happened in alphacarotene, betacarotene, and lutein of pumpkin. Apricot fruit dried at 60 and 70 °C	Ouyang et al. (2022) Piyarach et al. (2020) Albanese et al.		Air temperature: 60, 65, 70, and 75 °C Air velocity: 9 m/s Blanching: 90 s Air temperature: 40, 50, and 60 °C Air velocity: 1.5 m/s Air temperature: 40, 50, 60, and	during hot air drying was higher at 60 °C, while the differences in retention were not significant between 70 °C and 80 °C. Vitamin C of broccoli florets decreases rapidly as the drying temperature increases Vitamin C content of tomato and sweet pepper decreased with increasing temperature. Degradation of vitamin C content	Liu et al. (2019b) Kaur et al. (2020) Kumar et al.
	50–100 °C Air temperature: 60–100 °C Air temperature: 65 °C	temperature increased. The higher temperature, the higher loss of lycopene and betacarotene. Alpha- and betacarotenes in pumpkin slices were found more thermostable than dihydroxy xanthophylls. Losses over 50 % happened in alphacarotene, betacarotene, and lutein of pumpkin. Apricot fruit dried at 60 and 70 °C showed betacarotene losses of 20 % and 40 %,	Ouyang et al. (2022) Piyarach et al. (2020) Albanese et al.		Air temperature: 60, 65, 70, and 75 °C Air velocity: 9 m/s Blanching: 90 s Air temperature: 40, 50, and 60 °C Air velocity: 1.5 m/s Air temperature: 40, 50, 60, and 70 °C	during hot air drying was higher at 60 °C, while the differences in retention were not significant between 70 °C and 80 °C. Vitamin C of broccoli florets decreases rapidly as the drying temperature increases Vitamin C content of tomato and sweet pepper decreased with increasing temperature. Degradation of vitamin C content in spine gourd increases from 46.30 to 84.84 %	Liu et al. (2019b Kaur et al. (2020 Kumar et al.
	Air temperature: 60–100 °C Air temperature: 65 °C Air temperature: 65 °C	temperature increased. The higher temperature, the higher loss of lycopene and betacarotene. Alpha- and betacarotenes in pumpkin slices were found more thermostable than dihydroxy xanthophylls. Losses over 50 % happened in alphacarotene, betacarotene, and lutein of pumpkin. Apricot fruit dried at 60 and 70 °C showed betacarotene losses of 20 % and 40 %, respectively.	Ouyang et al. (2022) Piyarach et al. (2020) Albanese et al. (2013)		Air temperature: 60, 65, 70, and 75 °C Air velocity: 9 m/s Blanching: 90 s Air temperature: 40, 50, and 60 °C Air velocity: 1.5 m/s Air temperature: 40, 50, 60, and 70 °C Air velocity: 2 m/	during hot air drying was higher at 60 °C, while the differences in retention were not significant between 70 °C and 80 °C. Vitamin C of broccoli florets decreases rapidly as the drying temperature increases Vitamin C content of tomato and sweet pepper decreased with increasing temperature. Degradation of vitamin C content in spine gourd increases from 46.30 to 84.84 % with higher drying	Liu et al. (2019b Kaur et al. (2020 Kumar et al.
	Air temperature: 60–100 °C Air temperature: 65 °C Air temperature: 60 and 70 °C	temperature increased. The higher temperature, the higher loss of lycopene and betacarotene. Alpha- and betacarotenes in pumpkin slices were found more thermostable than dihydroxy xanthophylls. Losses over 50 % happened in alphacarotene, betacarotene, and lutein of pumpkin. Apricot fruit dried at 60 and 70 °C showed betacarotene losses of 20 % and 40 %, respectively. The highest	Ouyang et al. (2022) Piyarach et al. (2020) Albanese et al. (2013) Karabulut et al.		Air temperature: 60, 65, 70, and 75 °C Air velocity: 9 m/s Blanching: 90 s Air temperature: 40, 50, and 60 °C Air velocity: 1.5 m/s Air temperature: 40, 50, 60, and 70 °C Air velocity: 2 m/s	during hot air drying was higher at 60 °C, while the differences in retention were not significant between 70 °C and 80 °C. Vitamin C of broccoli florets decreases rapidly as the drying temperature increases Vitamin C content of tomato and sweet pepper decreased with increasing temperature. Degradation of vitamin C content in spine gourd increases from 46.30 to 84.84 % with higher drying temperatures.	Liu et al. (2019b) Kaur et al. (2020 Kumar et al. (2021)
	Air temperature: 60–100 °C Air temperature: 65 °C Air temperature: 65 °C	temperature increased. The higher temperature, the higher loss of lycopene and betacarotene. Alpha- and betacarotenes in pumpkin slices were found more thermostable than dihydroxy xanthophylls. Losses over 50 % happened in alphacarotene, betacarotene, and lutein of pumpkin. Apricot fruit dried at 60 and 70 °C showed betacarotene losses of 20 % and 40 %, respectively.	Ouyang et al. (2022) Piyarach et al. (2020) Albanese et al. (2013)		Air temperature: 60, 65, 70, and 75 °C Air velocity: 9 m/s Blanching: 90 s Air temperature: 40, 50, and 60 °C Air velocity: 1.5 m/s Air temperature: 40, 50, 60, and 70 °C Air velocity: 2 m/	during hot air drying was higher at 60 °C, while the differences in retention were not significant between 70 °C and 80 °C. Vitamin C of broccoli florets decreases rapidly as the drying temperature increases Vitamin C content of tomato and sweet pepper decreased with increasing temperature. Degradation of vitamin C content in spine gourd increases from 46.30 to 84.84 % with higher drying	Liu et al. (2019b) Kaur et al. (2020 Kumar et al.

Table 1 (continued)

Table 1 (continued)

Physicochemical attributes	Description	Findings	Reference	Physicochemical attributes	Description	Findings	Reference
	Air velocity: 1 m/s	during convective drying of cornelian cherry ranges between 79 % and 87 %. Lower drying temperatures (50 °C) result in greater ascorbic acid loss compared to higher temperatures (90 °C).			Air temperature: 38, 33, and 28 °C Relative humidity: 17, 20, and 32 %	isoamyl acetate, and butyl acetate showed a marked decrease after 24 h of drying, while elemicine levels remained stable. In banana, the highest percentage of loss for all compounds, excluding hexanal,	Saha et al. (2018)
Vitamin C	Air temperature: 50, 60, 70, 80, 90, and 100 °C Air velocity: 0.5 m/s	Increase in hot-air drying temperature from 50 °C to 100 °C led to a considerable decrease in ascorbic acid levels	Kittibunchakul et al. (2023)			occurred at 33 °C. Conversely, isoamyl acetate and isobutyl acetate exhibited their highest retention at 38 °C.	
	Air temperature: 60, 70, and 80 °C Air velocity: 1.5 m/s Blanching time: 2.5 and 5 min Slice thicknesses: 6, 8, and 10 mm	of maoberry fruits Increasing the blanching time from 0 to 5 min led to a decrease in vitamin C content except at 60 °C. Additionally, increasing the	Ozsan Kilic et al. (2023)		Air temperature: 60, 70, and 80 °C Air velocity: 1.5 m/s	Peppers dried at 70 °C or 80 °C had similar volatile flavor compounds, but both showed greater loss of these compounds compared to those dried at 60 °C	Ge et al. (2020)
	Air temperatures: 55, 60, 65, 70,	sample slice thickness resulted in increased vitamin C content of bitter gourd except at 80 °C. Relative humidity had little effect on	Farias et al. (1999)	Aroma	Air temperature: 60, 70, and 80 °C Air velocity: 1.5 m/s	Peppers dried at 70 °C or 80 °C had similar volatile flavor compounds, but both showed greater loss of these compounds compared to those	Ge et al. (2020)
	and 75 °C Relative humidity: 15, 20, 25, 30, 35, and 40 %	ascorbic acid retention at 55 °C and 60 °C, but higher temperatures (65 °C, 70 °C, and 75 °C) resulted in decreased retention with increased humidity.			Air temperature: 50 °C Air velocity: 0.45 m/s	dried at 60 °C Hot-air drying is a more effective method for producing the typical shiitake mushroom aroma compared to freeze drying and natural drying	Zhang et al. (2021a)
Aroma	Air temperature: 40, 50, and 60 °C Air velocity: 1.2 m/s Air temperature: 65 °C	At 50 °C, linalool, the primary aroma component of basil, exhibits a higher concentration compared to temperatures of 40 °C and 60 °C. In bell peppers, compounds such as	Barbieri et al. (2004) Luning et al. (1995)		Air temperature: 60, 70, and 80 °C	The highest trans- anethole content in dried star anise was observed at a drying temperature of 70 °C, while there was no significant difference in content between	Wen et al. (2020)
		(Z)-3-hexenal, (E)- 2-hexenal, octanal, (Z)-3-hexenol, linalool and (Z)-2- hexenal decreased or disappeared, while compounds like 2-methylpro- panal, 2-and 3- methylbutanal increased during			Air temperature: 45 and 60 °C	drying at 60 °C and 80 °C. Samples dried at 45 °C retained a greater amount of the fruity and sweet aromas characteristic of strawberry fruits compared to those dried at 60 °C.	Abouelenein et al. (2021)
	Air temperature: 40, 60, and 80 °C Air humidity:15 %, 5 %, and 3 % Air velocity: 2 m/ s	the drying process. A higher retention of aromatic compounds in banana was observed after drying at 40 °C. Isoamyl alcohol,	Boudhrioua et al. (2003)		Air temperature: 40, 50, 60, 70, and 80 °C	The aroma of S. granulatus varied with different drying temperatures. When dried at 60 °C, S. granulatus exhibited a more	Hou et al. (2022)

Table 1 (continued)

Physicochemical attributes	Description	Findings	Reference
		intense mushroom- like flavor.	
	Air temperature:	An increase in D-	Guo et al. (2022)
	35, 45, and 55 °C	carvone content	040 01 411 (2022)
		while decreasing D-	
		Limonene, cineole,	
		and 1-	
		caryophyllene with	
		higher drying	
	A ! 4	temperatures.	malas at an 4 makes
	Air temperature: 50, 60, and 70 °C	Drying strawberries at a	Tekgül and Erter (2022)
	50, 60, and 70 C	low temperature	(2022)
		(50 °C) preserved	
		the highest levels of	
		fresh strawberry	
		volatiles, whereas	
		at higher	
		temperatures	
		(60 °C and 70 °C),	
		the volatile profiles	
		of the dried strawberries	
		exhibited a similar	
		pattern.	
	Air temperature:	Increasing	Mishra et al.
	40, 50, and 60 °C	temperature leads	(2022)
	Air velocity: 1.5	to a reduction in	
	m/s	the most prevalent	
		components in	
		cardamom, such as	
		1,8-cineole and	
		α-terpinyl acetate.	

are lower in cost and less computationally intensive than imaging techniques.

- Hyperspectral and multispectral imagings could be more reliable techniques for delivering information on micronutrients because other techniques such as microwave, Terahertz, and Nuclear Magnetic Resonance (NMR) are highly sensitive to water molecules. Given the high water content in fruit vegetables, such a high sensitivity to water molecules can easily overshadow micronutrient signals. Hyperspectral and multispectral imaging can easily address this issue by identifying the spectral regions where water molecules do not absorb light, for example, the ultraviolet spectral region and the fingerprint spectral region of mid-infrared. Raman spectroscopy is also a potential technique because water molecules are associated with weak Raman signals.
- From the viewpoint of sensors integration into a dryer, hyperspectral (if snapshot), color, multispectral cameras, and electronic noses are technically simpler to be integrated. There are some reports on inline applications of other sensors, however their integration based on the current technology, is still more complex.
- Electronic noses and color cameras are relatively lower cost sensors for monitoring volatiles and color changes, respectively.
- Hyperspectral, nuclear magnetic resonance, X-ray micro-computed tomography, and Terahertz sensors are expensive. Multispectral imaging systems and microwave sensing, as affordable alternatives, must be further investigated.
- Microwave and Terahertz sensing techniques are highly sensitive to moisture content. They are both emerging techniques, and further research is required. However, microwave sensing is superior to be considered as an online monitoring tool because it is more costeffective.
- As a rule of thumb, multispectral cameras for micronutrients monitoring, microwave sensors for moisture content, particularly when surface hardening limits the light penetration, color cameras for

color monitoring, and electronic noses for volatiles can be considered as a fusion of sensors to be integrated into a hot-air dryer. It is noteworthy that microwave sensing is still emerging and future research is still required.

Table 2 summarizes the literature on sensors employed to monitor physicochemical attributes relevant to the drying process. Such realtime measurementds of physiochemical attributes together with drying condition (temperature, velocity, RH, ...) data are required to be fed into data-driven/machine learning algorithms, presented in section 4.1.5, with the aim of quantitative estimations of quality attributes. Such estimations will be used to adapt the fitting parameters of mathematical models (section 4.1) to improve their prediction accuracy.

4. High end model based process control

4.1. Models and approaches available

Models are described as mathematical representations of physical reality and real processes (Datta, 2016). Model-based studies have been used in different drying systems to gain better insight and understanding of the process, develop new designs, and optimize new and existing dryer designs (Defraeye, 2014). Models are alternatives to expensive and time-consuming experiments. Models can also be used to supplement experimental studies (Ramachandran et al., 2018). Drying is a complex process, and the detailed and accurate modeling of the process is complex. Modeling the drying process requires multidisciplinary knowledge, including transport phenomena (momentum, heat, and mass transfer), reaction kinetics, fluid and solid properties, and material science (Ramachandran et al., 2018). The drying process has been modeled using different approaches (Table 3). Depending on its accuracy and complexity, Khan et al. (2022a) categorized the available models into first, second, third, fourth, and fifth-generation models. First-generation models are basically constituted by empirical relationships; second-generation models include some physics-based knowledge of the empirical equations (semi-empirical); third-generation models are derived from physical principles; fourth-generation models describe the drying process at different spatial and time scales; and fifth-generation models integrate physics into data-driven relationships.

4.1.1. Empirical models

This type of model is developed by curve fitting the given expressions relating the process conditions and the relevant variables to the experimental data. For instance, the moisture ratio as a function of drying time, rate constant, and other constants. Well-known empirical drying models include Page, Modified Page, Lewis, Henderson and Pabis, modified Henderson and Pabis, Wang and Sing, logarithmic, two-term exponential, diffusion approach, Verma et al., and Midilli et al. (Khan et al., 2022a; Ramachandran et al., 2018), (Table 4). The basis for these model equations is Fick's second law for moisture diffusion. These models assume that the thickness of the product bed is a thin layer that is homogenous and neglects the geometrical shape of the product. It has been proven that these models are capable of predicting the drying process under experimental operating conditions (product initial moisture content, temperature, relative humidity, drying air flow rate, and bed thickness). Empirical models have been used to study the drying kinetics of different food and agricultural products such as maize (Asemu et al., 2020), chili (Getahun et al., 2021), rough rice (Sadaka, 2022), garlic (Chayjan et al., 2012), banana (Queiroz and Nebra, 2001), and potato (Akpinar et al., 2003). The main drawbacks of these types of models are: (i) the limited applicability and information about the flow, heat, and mass transfer characteristics (Prawiranto et al., 2021; Ramachandran et al., 2018) and (ii) their predictive capabilities are limited to the range of experimental conditions used to obtain the data required to estimate the model parameters (they are not valid for extrapolation). In addition, empirical models do not provide spatial or temporal

Table 2An overview of non-invasive sensors investigated in the drying process monitoring.

Purple-specified coopyam silces were analyzed during better with a property of the specific content of process of the process of the specific content of pro		Description	Findings	Reference
Puple-specified corroyon slices were analyzer during host eld of ying using hyperspectral langaging or shall always a continued to the prediction modifies of arbitalogs, or shall always a specified with high accuracy (Negurer 1 angas) (190 - 100 am) were captured of apple slices dried at air temperatures of 60° C and 79° C. Hyperspectral langaging (425-1700 mm) was employed to prodict the quality attributes of celeric during drying at temperature of 50, 60, and 70° C. Hyperspectral imaging (425-1700 mm) was employed to prodict the quality attributes of celeric during drying at temperature of 50, 60, and 70° C. Hyperspectral imaging (465-1700 mm) was employed to prodict the quality attributes of celeric during drying at modified to the celeric during drying attribute of the celeric during drying at modified to the celeric during drying attribute of the celeric during drying attribute of 200 - 100 and 200, 40, 200 and 2	Hyperspectral imaging (HSI)		wavelength accurately estimated shrinkage ($R^2\approx 0.95$, RMSE ≈ 4 %), vitamin C content ($R^2=0.92$, RMSE $=0.64$ mg/100 g FW), rehydration ratio ($R^2=0.67$, RMSE $=2.07$ %), and total phenolic compounds ($R^2=0.63$, RMSE $=$	Arefi et al. (2021)
Hyperspectral images (960–1010 any) were captured of apple slices dried at air temperatures of 50°C and 70°C C. Hyperspectral imaging (425–1700 and) was employed to predict the quality attributes of clearing during driving at temperatures of 50°C and 70°C. Hyperspectral images (980–1658 min) were captured for four vegetables during blot-air drying. Persimanon undergoing the drying process was monitored using the vegetable during blot-air drying. Persimanon undergoing the drying process was monitored using the vegetable during blot-air drying. Persimanon undergoing the drying process was monitored using the vegetable during blot-air drying. Persimanon undergoing the drying process was monitored throughout the host of 70°C vene monitored in the gene of 40°-900 and 8058 = 0.15 mg (64) gas 1°C close and 8058 = 0.04 mg (64) and 8058		hot-air drying using hyperspectral imaging across the	Wavelengths in the range of 951–999 nm significantly contributed to the prediction models for shrinkage,	Ndisya et al. (2021)
removable of the dispersion imaging (425-1700 nai) was employed to predict the quality attributes of celerias during drying at temperatures of 50, 60, and 70 °C. Hyperspectral imaging (985-1655 am) were captured for four vegetables during hot air drying. Persimmon undergoing the drying process was monitored using the spent age of 470-800 nm. Quality changes in carrots during drying at 50, 60, and 70 °C were monitored in the spectral region of 400 nm. Quality attributes of golden kiwi and purple carrot were monitored throughout the hot-air drying process. Low-field NMR vas used to monitor monito		Hyperspectral images (400-1010 nm) were captured of	The prediction model achieved an R-squared of 0.70 and RMSE of 0.040 for rehydration ratio, while moisture content was predicted with high accuracy (R-squared = 0.94, RMSE = 0.067 %). Shrinkage and color indices were	Shrestha et al. (2020)
Hyperspectral images (950-1655 mm) were captured for four vegetables during not-air drying, Persimmon undergoing the drying process was monitored using the spectral range of 470-900 mn. Quality changes in carrots during drying at 50, 60, and 70 °C were monitored in the operatin grain of 400-1010 mm. Quality attributes of banana slices were monitored throughout the microwave vacuum drying process. Quality attributes of golden kiwi and purple carrot were monitored throughout the hot-air drying process. Low-field NMR was used to monitor moisture content of fereze-haw pretreated loits not of listers and a small result in the 405-970 mm range were used to predict water fractions in mushrooms subjected to freeze-drying. Changes in the delectric properties of Chinese yam slices during microwave-vacuum drying processes. Low-field NMR at 23 MHz and spectral imaging within the 405-970 am range were used to predict water fractions in mushrooms subjected to foreze-drying. Changes in the delectric properties of Chinese yam slices during microwave-vacuum drying processes. Apple slices dried at various air temperatures were evaluated using NMR. The effects of moisture content, number of scans, and Resonance (NMR)/ Magnetic Resona		predict the quality attributes of celeriac during drying at	0.89 and RMSE = 0.04. Moisture content prediction achieved R-squared = 1.00 and RMSE = 0.77. Total phenolic content was predicted with R-squared = 0.49 and RMSE = 0.15 mg GAE gds $^{-1}$. Color indices were predicted with R-squared values ranging from 0.80 to 0.93 and	
monitored using the spectral range of 470-900 mm. Quality changes in carrots during drying at 50, 60, and 70 °C were monitored in the spectral region of 400-1010 nm. Quality attributes of banana silices were monitored throughout the microwave vacuum drying process. Quality attributes of golden kiwi and purple carrot were monitored throughout the hot-air drying process. Quality attributes of golden kiwi and purple carrot were monitored throughout the hot-air drying process. Low-field NIM so was used to monitor monitore of freeze-thaw pretreated lotus root slices exposed to monitor monitore of freeze-thaw pretreated lotus root slices exposed to monitor monitore drying process. Low-field NIM poperating at 232 MHz was used to monitor monitore of season and low-field nimbour or microwave-vacuum drying carrot slices. Low-field NIM poperating at 232 MHz was used to freeze-drying. Changes in the dielectric properties of Chinesey am slices during microwave-vacuum drying were investigated using NIM. Low-field NIM at 20 MHz was used to study changes in water content of garlic slees subjected to four different drying processes. Low-field NIM at 20 MHz was used to study changes in water content of garlic slees subjected to four different drying processes. Apple slices dried at various air temperatures were evaluated using NIM. The effects of mositure content, number of scans, and sample quantity on NIM accuracy for estimating moisture content, color, and shear force. The effects of mositure content, number of scans, and sample quantity on NIM accuracy for estimating moisture content of garlic slees subjected to four different drying processes. Furdicar Magnetic Resonance (NIMR)/ Magnetic Resonance (NIM			Moisture content was estimated with an R-squared of	Lin and Sun (2022)
yperspectral imaging (IRSI) Description of the spectral region of 400-1010 and property property of throughout the microwave vacuum drying process. Quality attributes of golden kiwi and purple carrot were monitored throughout the hot-air drying process. Low-field NiRI was used to monitor microwave-vacuum drying process. Low-field NiRI was used to monitor microwave-vacuum drying process. Low-field NiRI was used to monitor microwave-vacuum drying of carrot slices. Imaging (MRI) Low-field NiRI was used to monitor microwave-vacuum drying of carrot slices. Low-field NiRI was used to monitor microwave-vacuum drying of carrot slices. Low-field NiRI was used to monitor microwave-vacuum drying of carrot slices. Low-field NiRI at 23 MHz and spectral imaging within the 405-970 mm range were used to predict water fractions in mushrooms subjected to free-drying. Changes in the dielectric properties of Chinese yam slices during microwave-vacuum drying were hore decreasing. Changes in the dielectric properties of Chinese yam slices during microwave-vacuum drying were hore subjected to fore-different drying processes. Low-field NiRI at 20 MHz was used to study changes in water content of garlic slices subjected to four different drying processes. Low-field NiRI at 20 MHz was used to study changes in water content of garlic slices subjected to four different drying processes. Apple slices dried at various air temperatures were evaluated using NMR. The peaks in the T ₂ distribution were identified at col.1-10 ms, 10-80 ms, and 80-600 ms, corresponding to bound, immobility, and fire water, packed, and free water, pescretively. The production moless accurately captured the dielectric drovenages was the first of the peaks to shift leftward, and the overall signal peak decreased. Apple slices dried at various air temperatures were evaluated using NMR. At the early stage of drying, the number of scans had no effect. When moisture content dropped below 20 %, increasing the number of scans shad no effect. When moist		monitored using the spectral range of 470-900 nm.	squared of 0.857.	
Usperspectral imaging (HSI) Comparison of the discourage of throughout the microwave vacuum drying process. Quality attributes of golden kiwi and purple carrot were monitored throughout the hot-ait drying process.		70°C were monitored in the spectral region of 400–1010	0.90 and an RMSE of 8.16 %. Predictions for color and	Md Saleh et al. (2022)
Agentic Resonance (NMR)/ Magnetic Resonance		Quality attributes of banana slices were monitored	High prediction accuracy was achieved for moisture content (R-squared = 0.996). Good prediction accuracies were also obtained for hardness (R-squared = 0.886–0.927) and fracturability (R-squared =	Pu et al. (2018)
Low-field NMR was used to monitor moisture content of Resonance (NMR)/ Magnetic Resonance (NMR) (Procease-thaw pretreated lours root slices exposed to infrared and convection drying processes. Imaging (MRI) (MRI) (Procee-thaw pretreated lours root slices exposed to infrared and convection drying processes. Low-field NMR at 23 MHz and spectral imaging within the 405-970 mm range were used to predict water fractions in mushrooms subjected to freeze-drying. Changes in the dielectric properties of Chinese yam stices during microwave-vacuum drying were investigated using NMR. Low-field NMR at 20 MHz was used to study changes in water content of garlic slices subjected to four different drying processes. Apple slices dried at various air temperatures were evaluated using NMR. Apple slices dried at various air temperatures were evaluated using NMR. The effects of moisture content, number of scans, and sample quantity on NMR accuracy for estimating moisture content in carrot slices were investigated. Inaging (MRI) The use of NMR and MRI to analyze moisture variation in green plums during oven drying was explored. NMR operating at 30.0 MHz was used to investigate cellular water transfer in apple tissues during the drying processes. Distribution of T₂ identified the inflection point of water state instition. The signal peak associated with free water gradually decreased, while the peaks for trapped and bound water initially increased before decreasing. Both techniques, combined with learning algorithms, demonstrated promising results in estimating water fractions. The repetiction models accurately captured the dielectric changes, with R-squared values ≥ 0.921. Three peaks in the T₂ distribution were identified at 0.1–10 ms, 10–80 ms, and 80–600 ms, corresponding to bound, trapped, and free water molecules. The NMR parameters showed correlations with changes in moisture content, color, and shear force. At the early stage of drying, the number of scans had no effect. When moisture content dropped below 20			Machine learning algorithms accuratly estimated	Tayyab et al. (2025)
Low-field NMR operating at 23.2 MHz was used to monitor microwave-vacuum drying of carrot slices. Low-field NMR at 23 MHz and spectral imaging within the 405-970 mm range were used to predict water fractions in mushrooms subjected to freeze-drying. Changes in the dielectric properties of Chinese yam slices during microwave-vacuum drying were investigated using NMR. Low-field NMR at 20 MHz was used to study changes in water content of garlic slices subjected to four different drying processes. Apple slices dried at various air temperatures were evaluated using NMR. Apple slices dried at various air temperatures were evaluated using NMR. Apple slices dried at various air temperatures were evaluated using NMR. Apple slices dried at various air temperatures were evaluated using NMR. Apple slices dried at various air temperatures were evaluated using NMR. Apple slices dried at various air temperatures were evaluated using NMR. Apple slices dried at various air temperatures were evaluated using NMR. Apple slices dried at various air temperatures were evaluated using NMR. Apple slices dried at various air temperatures were evaluated using NMR. Apple slices dried at various air temperatures were evaluated using NMR. Apple slices dried at various air temperatures were evaluated using NMR. Apple slices dried at various air temperatures were evaluated using NMR. Apple slices dried at various air temperatures were evaluated using NMR. Apple slices dried at various air temperatures were evaluated using NMR. Apple slices dried at various air temperatures were evaluated using NMR. Apple slices dried at various air temperatures were evaluated using NMR. Apple slices dried at various air temperatures were evaluated using NMR. Apple slices dried at various air temperatures were evaluated using NMR. Apple slices dried at various air temperatures were evaluated using NMR. Apple slices dried at various air temperatures were evaluated using NMR. Are effect. When moisture content dropped below 20 %, increasing	Resonance (NMR)/	Low-field NMR was used to monitor moisture content of freeze-thaw pretreated lotus root slices exposed to	Distribution of T ₂ identified the inflection point of water	Zhang et al. (2022)
Low-field MMR at 23 MHz and spectral imaging within the 405-970 nm range were used to predict water fractions in mushrooms subjected to freeze-drying. Changes in the dielectric properties of Chinese yam slices during microwave-vacuum drying were investigated using NMR. Low-field MMR at 20 MHz was used to study changes in water content of garlic slices subjected to four different drying processes. Apple slices dried at various air temperatures were evaluated using NMR. Apple slices dried at various air temperatures were evaluated using NMR. Apple slices dried at various air temperatures were evaluated using NMR. Apple slices dried at various air temperatures were evaluated using NMR. Apple slices dried at various air temperatures were evaluated using NMR. Apple slices dried at various air temperatures were evaluated using NMR. Apple slices dried at various air temperatures were evaluated using NMR. Apple slices dried at various air temperatures were evaluated using NMR. Apple slices dried at various air temperatures were evaluated using NMR. Apple slices dried at various air temperatures were evaluated using NMR. Apple slices dried at various air temperatures were evaluated using NMR. Apple slices dried at various air temperatures were evaluated using NMR. Apple slices dried at various air temperatures were evaluated using NMR. Apple slices dried at various air temperatures were evaluated using NMR. Apple slices dried at various air temperatures were evaluated using NMR. Apple slices dried at various air temperatures were evaluated using NMR. Apple slices dried at various air temperatures were evaluated using NMR. At the early stage of drying, the number of scans had no effect. When moisture content dropped below 20 %, increasing the unmber of scans to 16 improved NMR performance. In the late stage of drying, a higher number of scans to 16 improved NMR performance. In the late stage of drying, a higher number of scans to 16 improved NMR performance. In the late stage of drying, a higher numbe	-	Low-field NMR operating at 23.2 MHz was used to	decreased as drying progressed, while the peaks for trapped and bound water initially increased before	Sun et al. (2019b)
during microwave-vacuum drying were investigated using NMR. Low-field NMR at 20 MHz was used to study changes in water content of garlic slices subjected to four different drying processes. Apple slices dried at various air temperatures were evaluated using NMR. Apple slices dried at various air temperatures were evaluated using NMR. Apple slices dried at various air temperatures were evaluated using NMR. Apple slices dried at various air temperatures were evaluated using NMR. Apple slices dried at various air temperatures were evaluated using NMR. Apple slices dried at various air temperatures were evaluated using NMR. Apple slices dried at various air temperatures were evaluated using NMR. Apple slices dried at various air temperatures were evaluated using NMR. Apple slices dried at various air temperatures were evaluated using NMR. Apple slices dried at various air temperatures were evaluated using NMR. Apple slices dried at various air temperatures were evaluated using NMR. Apple slices dried at various air temperatures were evaluated using NMR. Apple slices dried at various air temperatures were evaluated using NMR. Apple slices dried at various air temperatures were evaluated using NMR. Apple slices dried at various air temperatures were evaluated using NMR. Apple slices dried at various air temperatures were evaluated using NMR. Apple slices dried at various air temperatures were evaluated using beak decreased. Multi-exponential fitting of T₂ revealed four peaks corresponding to strongly bound, trapped, and free water molecules. The NMR parameters showed correlations with changes in moisture content dropped below 20 %, increasing the number of scans had no effect. When moisture content dropped below 20 %, increasing the number of scans had no effect. When moisture content dropped below 20 %, increasing the number of scans to 16 improved NMR performance. In the late stage of drying, a higher number of scans and a sample quantity of 1.0–1.5 g were recommended. The use of NMR and MRI to		the 405-970 nm range were used to predict water	Both techniques, combined with learning algorithms, demonstrated promising results in estimating water	Younas et al. (2021)
Low-field NMR at 20 MHz was used to study changes in water content of garlic slices subjected to four different drying processes. Apple slices dried at various air temperatures were evaluated using NMR. Apple slices dried at various air temperatures were evaluated using NMR. Apple slices dried at various air temperatures were evaluated using NMR. Apple slices dried at various air temperatures were evaluated using NMR. Apple slices dried at various air temperatures were evaluated using NMR. Apple slices dried at various air temperatures were evaluated using NMR. Apple slices dried at various air temperatures were evaluated using NMR. Apple slices dried at various air temperatures were evaluated using NMR. Apple slices dried at various air temperatures were evaluated using NMR. Apple slices dried at various air temperatures were evaluated using NMR. Apple slices dried at various air temperatures were evaluated using NMR. Apple slices dried at various air temperatures were evaluated using NMR. Apple slices dried at various air temperatures were evaluated using NMR. Apple slices dried at various air temperatures were evaluated using NMR. Apple slices dried at various air temperatures were evaluated using NMR. Apple slices dried at various air temperatures were evaluated using NMR. Apple slices dried at various air temperatures were evaluated using NMR. Apple slices dried at various air temperatures were evaluated using not strongly bound, lightly bound, trapped, and free water molecules. The NMR perameters showed correlations with changes in moisture content dropped below 20 %, increasing the number of scans to 16 improved NMR performance. In the late stage of drying, a higher number of scans and a sample quantity of 1.0–1.5 g were recommended. Angentic Resonance At the early stage of drying, the number of scans to 16 improved NMR performance. In the late stage of drying, a higher number of scans and a sample quantity of 1.0–1.5 g were recommended. Apple slices dried at various air temperatures		during microwave-vacuum drying were investigated	* *	Li et al. (2019)
Apple slices dried at various air temperatures were evaluated using NMR. Apple slices dried at various air temperatures were evaluated using NMR. Apple slices dried at various air temperatures were evaluated using NMR. And free water molecules. The NMR parameters showed correlations with changes in moisture content, color, and shear force. At the early stage of drying, the number of scans had no effect. When moisture content dropped below 20 %, increasing the number of scans to 16 improved NMR performance. In the late stage of drying, a higher number of scans and a sample quantity of 1.0–1.5 g were recommended. Amount of the exterior of carrot cubes during the drying process. The use of NMR and MRI to analyze moisture variation in green plums during oven drying was explored. NMR operating at 300 MHz was used to investigate cellular water transfer in apple tissues during the drying corresponding to strongly bound, lightly bound, trapped, and free water molecules. The NMR parameters showed correlation from the interior of the early stage of drying, the number of scans had no effect. When moisture content dropped below 20 %, increasing the number of scans to 16 improved NMR performance. In the late stage of drying, a higher number of scans and a sample quantity of 1.0–1.5 g were recommended. NMR/MRI depicted moisture migration from the interior to the exterior of carrot cubes during the drying process. Signal peaks of A ₂₃ (representing free water) and A ₂ total (representing all water states) showed correlation coefficients of 0.958 and 0.936 with water content changes, respectively. Water transfer from the intracellular to intercellular space was primarily caused by cell rupture. Khan et al. (2018)		Low-field NMR at 20 MHz was used to study changes in water content of garlic slices subjected to four different	0.1–10 ms, 10–80 ms, and 80–600 ms, corresponding to bound, immobilized, and free water, respectively. Prolonged drying caused the peaks to shift leftward, and	Chen et al. (2020b)
At the early stage of drying, the number of scans had no sample quantity on NMR accuracy for estimating moisture content in carrot slices were investigated. Imaging (MRI) At the early stage of drying, the number of scans had no effect. When moisture content dropped below 20 %, increasing the number of scans to 16 improved NMR performance. In the late stage of drying, a higher number of scans and a sample quantity of 1.0–1.5 g were recommended. - NMR/MRI depicted moisture migration from the interior to the exterior of carrot cubes during the drying process. The use of NMR and MRI to analyze moisture variation in green plums during oven drying was explored. NMR operating at 300 MHz was used to investigate cellular water transfer in apple tissues during the drying was primarily caused by cell rupture. At the early stage of drying, the number of scans had no effect. When moisture content dropped below 20 %, increasing the number of scans to 16 improved NMR performance. In the late stage of drying, a higher number of scans had no effect. When moisture content dropped below 20 %, increasing the number of scans to 16 improved NMR performance. In the late stage of drying, a higher number of scans to 16 improved NMR performance. In the late stage of drying, the number of scans to 16 improved NMR performance. In the late stage of drying, a higher number of scans to 16 improved NMR performance. In the late stage of drying, a higher number of scans to 16 improved NMR performance. In the late stage of drying, a higher number of scans to 16 improved NMR performance. In the late stage of drying, a higher number of scans to 16 improved NMR performance. In the late stage of drying, a higher number of scans to 16 improved NMR performance. In the late stage of drying, a higher number of scans to 16 improved NMR increasing the number of scans to 16 improved NMR increasing the number of scans to 16 improved NMR increasing the number of scans to 16 improved NMR increasing the number of scans to 16 improved NMR increasing the n			Multi-exponential fitting of T_2 revealed four peaks corresponding to strongly bound, lightly bound, trapped, and free water molecules. The NMR parameters showed correlations with changes in moisture content, color, and	Kamal et al. (2019)
to the exterior of carrot cubes during the drying process. The use of NMR and MRI to analyze moisture variation in green plums during oven drying was explored. Signal peaks of A ₂₃ (representing free water) and A_total (representing all water states) showed correlation coefficients of 0.958 and 0.936 with water content changes, respectively. NMR operating at 300 MHz was used to investigate cellular water transfer in apple tissues during the drying was primarily caused by cell rupture. Khan et al. (2018)	Resonance (NMR)/ Magnetic Resonance	sample quantity on NMR accuracy for estimating	At the early stage of drying, the number of scans had no effect. When moisture content dropped below 20 $\%$, increasing the number of scans to 16 improved NMR performance. In the late stage of drying, a higher number of scans and a sample quantity of 1.0–1.5 g were	Sun et al. (2021a)
green plums during oven drying was explored. (representing all water states) showed correlation coefficients of 0.958 and 0.936 with water content changes, respectively. NMR operating at 300 MHz was used to investigate cellular water transfer in apple tissues during the drying was primarily caused by cell rupture. (representing all water states) showed correlation coefficients of 0.958 and 0.936 with water content changes, respectively. Water transfer from the intracellular to intercellular space Khan et al. (2018) was primarily caused by cell rupture.		-		Gong et al. (2020)
cellular water transfer in apple tissues during the drying was primarily caused by cell rupture.		-	(representing all water states) showed correlation coefficients of 0.958 and 0.936 with water content	Zhu et al. (2021)
		cellular water transfer in apple tissues during the drying	-	Khan et al. (2018)

Table 2 (continued)

Sensor	Description	Findings	Reference
	NMR and MRI were utilized to investigate the drying kinetics of mulberries subjected to hot-blast air drying.	Water migration in its various states was traceable using NMR and MRI, with NMR/MRI data showing strong	Li et al. (2021b)
	-	correlations with quality attributes. MRI revealed enhanced water migration in kiwi slices at	Liu et al. (2019a)
	NMR and MRI were employed to monitor the pulsed vacuum drying of blueberries.	higher ultrasonic power levels. MRI revealed that the higher water transfer during the early stage of drying was linked to the enlargement and	Liu et al. (2021)
	NMR/MRI was used for real-time monitoring of moisture content in potato and broccoli stalks.	interconnection of pores. NMR/MRI signals showed a strong correlation with moisture content (R-squared >0.90). The detection limits were 11 % for NMR and 20 % for MRI.	Jiang et al. (2019)
	NMR was used to determine the safe water activity levels in apple, carrot, white cabbage, cauliflower, and radish.	T_{21} proved to be a reliable indicator of safe water activity (below 0.6).	Chitrakar et al. (2019)
	NMR was used to investigate moisture transfer in banana slices subjected to contact ultrasound-enhanced far-	NMR analysis revealed a gradual decrease in free water, while trapped water initially increased before decreasing.	Shi et al. (2020)
Nuclear Magnetic	infrared radiation drying. NMR data were collected for carrot, banana, and an	Bound water showed no significant change. The models estimated moisture content with an R-squared	Sun et al. (2019c)
Resonance (NMR)/ Magnetic Resonance Imaging (MRI)	edible fungus during microwave-vacuum drying. Low-field NMR was used to monitor moisture content and its states in raspberries during pulse-spouted microwave	of 0.9955 and an RMSE of 0.0211. Both free and trapped water decreased significantly, while bound water showed no significant change.	Sun et al. (2021c)
	freeze drying. NMR was used to determine the drying end-point of	The observation of a major peak at a relaxation time of 1	Chitrakar et al. (2021)
	asparagus leaves, stems, and roots. Various pretreatments enhanced the far-infrared drying	ms indicated that water activity was below 0.6. Pretreatments accelerated the shift of T ₂ towards shorter	Chao et al. (2022)
	of pumpkin. –	relaxation times. NMR showed potential for estimating flavor changes in garlic and ginger subjected to thermal processing.	(Sun et al., 2019d, 2021b)
Microwave sensing	A review was presented on various antenna sensors and microwave-based methods used to measure the moisture content of grains and minerals.	The S-parameter was found to be more suitable for measuring moisture content than dielectric constant and impedance methods. Frequency selective surface (FSS) was identified as the most suitable portable sensor.	Javanbakht et al. (2021a)
	A review was conducted on the dielectric properties of various foodstuffs.	The dielectric properties were found to depend on several factors, including frequency and temperature.	Bogale Teseme and Weldemichael Weldeselassie (2020)
	The moisture content of paddy rice was correlated with microwave attenuation and phase changes at 3.00 GHz. Ambient temperature was included as an input in the prediction models to compensate for its effects.	The moisture content was predicted with low error.	Liu et al. (2022)
	prediction models to compensate for its effects. A new frequency selective surface (FSS) antenna was used to measure moisture content (10–25 %) in barley grains.	The sensor was sensitive to small variations in moisture content.	Javanbakht et al. (2021b)
	Horn antennas operating at 10.5 GHz were used to measure the moisture content of rice and corn.	Higher moisture content led to increased wave attenuation.	Li et al. (2021a)
	Tomographic imaging systems were used to monitor the moisture content of corn kernels during fluidized drying.	Microwave tomography demonstrated greater sensitivity to changes in moisture content compared to capacitance tomography.	Lin et al. (2022)
Terahertz sensing (THz)	The THz technique was reviewed for food safety and quality and soil sensing was also part of the review.	to the spectroscopy techniques even though it is a promising method. Thickness dependency, scattering effect, particle size and surface roughness effects and high moisture content can challenge the THz technique.	Khushbu et al. (2022)
	A review of THz technology was presented, highlighting its potential for monitoring moisture content during food drying, measuring sugars in osmotically dehydrated foods, analyzing proteins and amino acids in dried	The strong absorption of water molecules in the THz region limits the ability to monitor other chemical components during the drying process.	Zhang et al. (2021b)
	products, and detecting foreign bodies in dried foods. The application of THz technology was reviewed for determining carbohydrate concentrations in liquids and powders, detecting foreign bodies and chemical residues in carbohydrate-based foods, monitoring carbohydrate fermentation, and assessing carbohydrate crystallinity.	THz application in dietary carbohydrates is still in its infancy. Its ability to measure the thickness and refractive index of the food matrix offers an advantage over NIR spectroscopy. However, the high initial cost and dependency on sample thickness remain significant challenges.	Li et al. (2023)
	Water loss of Ginkgo seeds under ambient temperature was monitored in the frequency range up to 7 THz.	Seeds with higher moisture content showed higher absorption coefficients.	Gong et al. (2022)
	Kiwi slices exposed to a combination of freeze-drying and microwave-vacuum drying methods were investigated	THz signal amplitude was found to be related to the slice structure.	Huang et al. (2021)
	using THz imaging. In-situ microwave-vacuum drying of beef slices was conducted using the THz imaging technique.	Calibration models accurately predicted the changes in moisture content.	Ren and Sun (2022)
	In-situ microwave-vacuum drying of beef and carrot slices was carried out using THz-TDS.	Moisture content was predicted with an R-squared value of 0.995 and an RMSE of 0.0162.	Ren et al. (2023)
	Spectral information of pork slices and leaves exposed to the drying process was captured in the frequency range of	Low error estimation was achieved for moisture content.	Borovkova et al. (2018)
	0.1–0.9 THz.		(continued on next page)

Table 2 (continued)

Sensor	Description	Findings	Reference
Color/RGB camera	Microwave drying was studied at different power levels and slice thicknesses, and changes in color kinetics were	The study successfully determined variations in color kinetics in the CIELab space based on CVS data, which	Nagvanshi et al. (2021)
	monitored using a color camera. RGB color imaging was conducted during drying of apples and carrots.	fitted well to first-order and zero-order models. The quality parameters of apples and carrots during the drying process were successfully detected based on color attributes.	Sturm et al. (2018)
	The computer-vision system effectively monitored quality degradation during the three-stage drying of ginseng at 50 $^{\circ}\text{C}.$	The quality aspects such as actual moisture content and quality degradation of roots were monitored using a computer-vision system with high accuracy, achieving an error range of 8–14 % in moisture content estimation at 95 % confidence.	Martynenko (2006)
	The food drying process was analyzed using computer vision with three different heat sources while capturing images with RGB cameras during the process.	The study found that the lowest errors in training and test data were achieved using resistance drying and infrared methods to control the drying process. Resistance values showed the best results based on R-squared values.	Ozden (2022)
	RGB camera imaging was used to monitor the quality of turmeric during the drying process.	Based on color information extracted from images in terms of CIELab values, moisture and product quality were successfully monitored.	Sharma et al. (2019)
	The intervention in the study involved drying carrot slices at 35 $^{\circ}$ C for 36 h using a smart dryer equipped with a computer vision system and a load cell.	The color camera proved effective in monitoring drying processes, with linear models showing high prediction accuracy for moisture content and minimal impact of	Moscetti et al. (2020)
	Pea shrinkage was studied during fluidized bed drying.	blanching treatment on model performance. Offline color imaging data explored shrinkage with lower error, while real-time measurements showed slight deviations.	Theonye et al. (2020)
	Quality changes in carrot slices were studied during convective air drying.	The computer vision system effectively measured color changes and shrinkage, achieving a good RMSE range of 0.005–0.007.	Chakravartula et al. (2023)
Color/RGB camera	The application of a color camera for quality monitoring of apple slices during drying was investigated.	Morphological properties, moisture content, and CIELab values were measured with high efficiency, achieving R-squared values above 0.98 and low error.	Raponi et al. (2022)
	The moisture ratio of thin layers of date fruit was analyzed based on real-time color attributes and environmental conditions during the drying process.	Moisture content was estimated with high accuracy using online image attributes and machine learning techniques.	Keramat-Jahromi et al. (2021)
X-ray micro-computed tomography (XCT)	XCT was used to study the freeze-drying process of maltodextrin solutions in situ. The resolution was 3 μ m, and the measurement time was approximately 1.4 h.	A new method was presented to study microstructural changes during freeze-drying and analyze drying kinetics in situ using grayscale images obtained by XCT.	Gruber et al. (2021)
	This study investigates how the spin freezing rate affects the characteristics of dried product layers in spin freezedrying. Resolution: 4.5–8 μm Measurement time: $\sim\!0.7h$	Utilizing high-resolution XCT, this research explores the relationship between spin-freezing rates and pore size, shape, mass transfer resistance, and solid-state properties of dried product layers. The results indicate that slower spin-freezing rates produce highly tortuous structures with greater mass-transfer resistance, while faster spin-freezing rates lead to lamellar structures with lower tortuosity and resistance.	Lammens et al. (2021)
	This study investigates the impact of hot-air drying (HAD) on the structure of dried fruits and vegetables, with a particular focus on crust formation. Using a threestep process involving HAD, freezing, and freeze-drying, the development of a crust on carrot discs is examined. Resolution: $14~\mu m$ Measurement time: ~ 70 min	Results reveal that crust thickness increases significantly during HAD, with crust formation beginning before the relative moisture content reaches 0.5. XCT measurements provide detailed analysis of the crust structures formed during HAD.	Siebert et al. (2018)
X-ray micro-computed tomography (XCT)	This study examines the microstructure of spray-dried particles—commonly used in amorphous solid dispersions to enhance the performance of poorly water-soluble drugs—using XCT and other imaging techniques. Resolution: 0,8 µm Measurement time: 5h	Higher outlet temperatures during spray drying produce more spherical hollow particles with thinner walls, while lower temperatures generate raisin-like particles with thicker walls. Artificial intelligence–facilitated XCT image analysis enables quantitative assessment of thousands of individual particles, revealing envelope density as a sensitive indicator of process changes. Additionally, particle wall thickness correlates with tensile strength, highlighting potential implications for particle engineering and drug product optimization.	Xi et al. (2020)
	In-situ XCT was utilized to observe microstructure development during freeze-drying of a dextrin solution using a specially designed freeze-drying stage. Resolution: ~3 µm Measurement time: 30s	XCT imaging captured frozen and dried microstructures, revealing an increase in ice crystal size and boundary formation between ice and freeze-concentrated phases after freezing annealing. Pore microstructures formed during freeze-drying replicated the original ice structures and generated new pores as water was removed, especially in non-annealed samples. Image analysis showed thicker pore walls in annealed samples compared to non-annealed ones, suggesting that annealing not only reduces drying time by modifying ice crystal morphology but also prevents structural deformation of glassy phases, thereby preserving product quality.	Nakagawa et al. (2018)
		preserving product quality.	
	The study focuses on evaluating X-ray microtomography (XCT) as a method for characterizing the matrix of freeze-	XCT provides uniform contrast and simplifies analysis. Results reveal two main structures: large pores separated	Palmkron et al. (2023)

Table 2 (continued)

Sensor	Description	Findings	Reference
	dried materials. Resolution: 0,657 μm	by thin walls and a finer, honeycomb-like structure. Despite varying drying conditions, these structures show	
	Measurement time: 9h	minimal variation.	Y 1 (0010)
K-ray micro-computed	This study examines the effects of freeze-drying,	The study finds that freezing rate influences ice crystal size	Voda et al. (2012)
tomography (XCT)	blanching, and freezing rate pre-treatments on the microstructure and rehydration properties of winter	and pore formation, while blanching does not affect pore size distribution. Rehydration leads to the formation of a	
	carrots using various imaging techniques.	porous network rather than restoration of cellular	
	Resolution: 4 µm	compartments. Blanching followed by fast freezing helps	
	Measurement time: 50 min	preserve more of the native cell wall morphology.	
	Advanced X-ray Microscopy (XRM) combined with	The study reveals that normalized diffusion coefficients,	Pu et al. (2023)
	mathematical models correlates microstructure, drying	derived from 3D microstructure reconstructions, correlate	
	kinetics, and reconstitution time.	with the solid content of pre-lyophilization solutions,	
	Resolution: 2 µm Measurement time: 4–8 h	influencing pore size and volume. While mass transfer models accurately describe drying kinetics, formulation	
	weastirement time. 4–0 ii	ingredients affect mass transfer mechanisms, complicating	
		reconstitution process modeling. X-ray microscopy	
		combined with mathematical models provides valuable	
		insights into lyophilization processes.	
	This study introduces a method to estimate mass transfer	Solid concentration and annealing above Tg' significantly	Foerst et al. (2019)
	rates during primary drying using XCT measurements of	influence pore size and drying rates. This highlights	
	freeze-dried cakes. Resolution: 1 µm	annealing as an effective method to accelerate primary drying, the most time-consuming step in lyophilization.	
	Measurement time: ~2,5h	drying, the most time-consuming step in Tyophinzation.	
	This study investigates the use of supercritical carbon	Comparisons with air drying reveal differences in drying	Brown et al. (2008)
	dioxide (scCO2) for moisture removal from cylindrical	kinetics and mechanisms. Microstructural analysis using	
	carrot pieces, examining the effects of temperature and	X-ray microtomography and light microscopy shows that	
	ethanol as a co-solvent at 20 MPa pressure. The results	carrots dried with supercritical fluids better retain their	
	are compared with those of hot air drying.	shape than those dried by air. Additionally, ethanol-	
	Resolution: 5 µm Measurement time: not given	modified scCO2 drying produces less dense structures and improves rehydrated textural properties.	
X-ray micro-computed	This study presents an analytical method employing four-	By incorporating these Rp values into mechanistic models,	Vanbillemont et al. (2020
tomography (XCT)	dimensional micro-computed tomography (4D-XCT) to	the drying time distribution of spin-frozen vials can be	, (2-2-
	assess differences in intra-vial mass transfer resistance	predicted and experimentally verified using thermal	
	(Rp) of dried products during freeze-drying.	imaging. Additionally, 4D-XCT enables measurement of	
	Resolution: 30 µm	key freeze-drying parameters, such as sublimation front	
	Measurement time: ∼3 min	movement and frozen product layer thickness, offering detailed process insights. Overall, the study accurately	
		predicts primary drying time variations in individual vials	
		using 4D-XCT, with validation provided by thermal	
		imaging.	
Laser light backscattering	The mango drying process was monitored at wavelengths	The model predicting moisture content at 635 nm was the	Bai et al. (2021)
imaging (LLBI)	of 450, 520, and 635 nm.	most accurate.	
	Banana slices dried at temperatures ranging from 50 °C to	The strong NIR absorption spectrum shows wavelength	Siyum et al. (2023)
	70 °C were monitored in the spectral range of 740–1700 nm.	shifts between 1064 and 1416 nm.	
	Images of ham slices were captured during the drying	The study revealed that a red laser (635 nm) is more	Fulladosa et al. (2017)
	process.	practical than a green laser (532 nm). A decrease in	
	•	scattering area was observed only when the water content	
		decreased.	
	A 670 nm laser diode was used to monitor banana slices	Moisture content was significantly correlated with	Romano et al. (2008)
	for moisture content.	backscattered area.	O (0010-)
	Sweet potato slices were monitored for moisture content	Drying temperature and time had a significant effect on the parameters obtained from combined computer vision	Onwude et al. (2018a)
	and color using a combination of LLBI and computer vision.	and backscattering imaging.	
	Apple slices were monitored for moisture content at	These wavelengths were found to be highly correlated	Arefi et al. (2023b)
	wavelengths of 635 nm, 980 nm, and 1450 nm.	with changes in moisture content.	
Raman spectroscopy	The feasibility of using in situ Raman spectroscopy for	Raman spectroscopy effectively tracked the reduction of	Braeuer et al. (2017)
	online monitoring of supercritical carbon dioxide (SC-	water content and changes in the fruit matrix structure	
	CO2) drying processes in mango and persimmon fruits	during drying.	
	was investigated.	The hydration state of risedronate was successfully	Hausman et al. (2005)
	The solid-state changes of Risedronate sodium granules during lab-scale Fluidized Bed Drying (FBD) are	monitored using Raman spectroscopy, enabling effective	Hausiliali et al. (2003)
	monitored, a crucial aspect for assessing the stability and	identification of the process endpoint while ensuring	
	efficacy of pharmaceutical formulations.	product quality.	
	Three-dimensional maps of particle concentration and	The composition of materials and particle distribution	Walker et al. (2009)
	chemical structure in a fluidized bed were generated	within a fluidized bed were successfully monitored within	
	using Raman spectroscopy.	a 10-s interval.	
	Raman spectroscopy was used to evaluate the carotenoid	A strong correlation between Raman spectroscopy results	Carvalho et al. (2019)
	content in processed <i>Bunchosia glandulifera</i> . Carotenoid degradation in sweet potatoes subjected to	and carotenoid content was clearly demonstrated. Raman intensity showed a strong correlation with	Sebben et al. (2018)
	hot air and microwave drying processes was investigated.	carotenoid degradation.	Seppen et al. (2016)
Multispectral Imaging	A 980 nm LED array combined with a monochrome	The system accurately monitored the moisture content of	Arefi et al. (2023a)
(MSI)	camera was integrated into a hot air dryer.	apple slices.	
	Multispectral imaging and NMR were used to monitor the	Free, immobilized, bound, and total water contents were	Younas et al. (2021)
	freeze-drying process of shiitake mushrooms.	predicted with R ² values above 0.85 and RMSE below	
		18.13 %.	
			(continued on next page)

Table 2 (continued)

Sensor	Description	Findings	Reference
	The study aimed to evaluate the quality of carrot slices subjected to a drying process.	Moisture content (R-squared = 0.953, RMSE = 0.0902 %) and shrinkage (R-squared = 0.942, RMSE = 0.0808 %) were accurately predicted.	Yu et al. (2020)
	Moisture and carotenoid contents of carrot slices were monitored.	A model developed using seven optimal wavelengths achieved coefficients of determination of 0.991 and 0.968, and relative percentage deviations of 10.318 and 5.337 for moisture content and carotenoid, respectively.	Long et al. (2021)
	Spectral images of mango slices were captured during drying at temperatures ranging from 40 $^{\circ}$ C to 80 $^{\circ}$ C and air humidities between 5 % and 30 %.	Soluble solids content, pH value, and moisture content were accurately predicted.	Jödicke et al. (2020)
Electronic nose (E-nose)	Detection of volatile organic compounds during hot air drying of mint.	E-nose based principal component analysis successfully reflected variations in volatile organic compounds.	Kiani et al. (2018)
	Flavor analysis of golden pompano fillets subjected to different drying methods.	Volatile compounds of samples dried by four different methods were clearly differentiated using E-nose and E- tongue systems.	Zhang et al. (2019)
	Determination of volatile compounds in shiitake mushrooms at different drying stages.	E-nose successfully classified samples according to different drying stages.	Zhang et al. (2020)
	Assessment of volatile profiles in green tea during the drying process.	Gas-phase electronic nose captured the dynamic changes occurring under different drying conditions.	Yang et al. (2022)
	The composition and aroma profiles of button mushrooms were monitored at different drying stages using a metal-oxide semiconductor (MOS) sensor.	Button mushroom samples subjected to different drying durations were successfully discriminated.	Pei et al. (2016)
	Aroma assessment of garlic subjected to different drying methods was conducted.	Samples subjected to different drying methods were successfully discriminated using an electronic nose.	Makarichian et al. (2021)

information about the drying variables (Prawiranto et al., 2021).

4.1.2. Semi-empirical models

These models integrate physics-based knowledge within the empirical relationships described in the previous section to minimize their drawbacks (Khan et al., 2022a; Putranto et al., 2011). The evaporation of moisture during drying was modeled as a first-order reaction with activation energy, whereas condensation was modeled as a zero-order reaction. Compared to the empirical models, these models produced slightly better results. However, these models are still dependent on product type and drying conditions and are still unable to take into account the complete physics of the drying process (Khan et al., 2022a). Semi-empirical models have been applied to study the drying characteristics of different products such as wood particles (Kharaghani et al., 2019), carrots (Yang et al., 2021), and kiwi (Chen et al., 2001). The relevant semi-empirical model equations could be found in Yang et al. (2021).

4.1.3. Physics based models

These are advanced drying models that are derived from the fundamental laws of physics, mathematics, chemistry, and biology, and are capable of capturing real drying phenomena. Physics-based models have been developed based on the conservation of mass, energy, and momentum, Navier-Stokes equations for fluid flow, and Newton's law of motion (Khan et al., 2022a). The details of the air and product side drying model equations can be found in Delele et al. (2023).

These models could provide a high-resolution spatial and temporal distribution of the drying parameters (temperature, relative humidity, moisture content, air velocity, and product quality). The information could be used for a fundamental understanding of the drying process, optimization of the design and operating conditions of the dryer, and the development of new dryer designs (Khan et al., 2022a; Prawiranto et al., 2021). The approach includes Computational Fluid Dynamics (CFD) and CFD-Discrete Element method (DEM). CFD is the most commonly applied physics-based modeling technique for drying processes study (Defraeye, 2014; Ramachandran et al., 2018). CFD has been used to study the drying phenomena of different products and dryers. For instance, CFD has been applied to study apricot drying using an infrared dryer (Aktas et al., 2017), soya meal drying using a fluidized bed (Da Silva et al., 2012), convective drying of quince slices (Tzempelikos et al., 2015), sweet potato drying using a combined convective infrared dryer (Onwude et al., 2018b), rough rice drying using a convective mixed-flow

dryer (Delele et al., 2023), moist object drying (Chandramohan, 2016), and ellipsoidal particle drying in a fluidized bed dryer where CFD is coupled with DEM (Handayani et al., 2023). The multiscale, multiphysics, and multiphase nature of the drying process makes it challenging to develop purely physics-based models. Therefore, some commonly used assumptions are still made during the derivation of physics-based models in the macroscale drying process (Defraeye, 2014). There has been a recent development in multiphase physics-based drying models, considering the irregular pore space inside the product, capillary and binary diffusion of liquid, and mass transfer of the vapor (Lu et al., 2021). However, this model is still incapable of capturing microscale transport (Khan et al., 2020).

4.1.4. Multiscale models

Drying is associated with a transport process that occurs on different spatial and temporal scales (Defraeye, 2014). Multiscale drying models are the most advanced physics-based models used to study the transport of water from cellular (microscale) to tissue (macroscale) scales (Khan et al., 2020). Different cellular environments (intercellular, intracellular, and cell wall) contain different amounts of water, resulting in the transport of water from different cellular environments (Khan and Karim, 2017). In addition, different cells exhibit different water transport characteristics. These inhomogeneous water transport characteristics at the microscale (cellular) level affect macroscale water transport characteristics. It is extremely important to consider the microscale properties and transport characteristics to fully understand the drying process, accurately predict the drying process, and optimize the full-scale dryer. Because multiscale models describe transport at both micro and macro levels, the number of assumptions made during the derivation is lower than that of the previous alternatives. Although these models provide better insight and high-resolution (spatial and temporal) information about the drying process, their development and solutions are challenging and computationally demanding (Khan et al., 2020). Despite these challenges, encouraging studies have been reported on the multiscale modeling of drying and dehydration processes (Aregawi et al., 2014; Ho et al., 2011; Welsh et al., 2021).

4.1.5. Machine learning models for spatial and temporal dynamics

The application of machine learning models from high-dimensional sensor data to food-drying processes has emerged as a key strategy for developing Digital Twins that enable real-time monitoring and control. These models leverage various data structures ranging from two-

Table 3 An overview of recent studies and the corresponding models and approaches in the drying process.

Model	Description	Findings	References
Empirical model	The impact of rice layer thickness on drying rate and moisture diffusivity was studies.	Drying rate and moisture diffusivity increased with an increase in air temperature and a decrease in layer thickness. Page model produced the	Sadaka (2022)
	The effect of maize load and mixing time interval on drying time of solar bubble dryer was investigated.	best fit. Drying time decreased with a decrease in product load and mixing interval. The study recommended Verma et al. and diffusion approach models.	Asemu et al. (2020)
	Used double tunnel solar dryer and investigated collector efficiency, carbon footprint and the effect chili variety and layer density on drying time.	There was an improvement in drying rate compared to sun drying and a significant CO2 mitigation because of the solar dryer. Modified Henderson and Pabis and Verma et al. models were recommended.	Getahun et al. (2021)
	The effect of drying air temperature on drying time, moisture diffusivity and specific energy consumption during garlic drying using fluidized and semi fluidized bed dryer was investigated.	An increase in drying air temperature increased the drying rate, moisture diffusivity and specific energy consumption. Page model gave the best fit.	Chayjan et al. (2012)
Semi- empirical model	The applicability of reaction engineering approach in predicting temperature and moisture distributions of shrinkable food (carrot) at different drying temperature was evaluated.	The model was capable of predicting temperature and moisture distribution with R2 > 0.98. Drying rate increased with drying temperature.	Yang et al. (2021)
	The accuracy of reaction engineering approach in predicting drying behaviour of kiwifruit was assessed.	The model was capable of predicting the moisture content with R2 > 0.93. Drying rate increased with temperature.	Chen et al. (2001)
Physics based model	assessed. The study used CFD model to steady the heat and mass transfer characteristics during apricot drying using Infrared dryer, and analyzed the effect of product temperature and air	cemperature. CFD model was capable of predicting drying airflow velocity, temperature and product moisture content with an acceptable accuracy. The highest energy efficiency was obtained for the	Aktaş et al. (2017)

Model	Description	Findings	References
	velocity on dryer efficiency.	highest temperature and lowest air	
	Multiphase CFD	velocity. The model was	Da Silva et al.
	model was used to	capable of	(2012)
	predict the drying	predicting the	
	behaviour of	transient	
	soybean meal using	temperature,	
	a fluidized bed dryer.	velocity and porosity	
	drycr.	distributions.	
		Temperature was	
		the variable with	
		the most significant	
		effect on the drying characteristics.	
Physics	CFD model was	The time evolution	Tzempelikos et al.
based	used to study the	of temperature and	(2015)
model	heat and mass	moisture content	
	transfer process	was well predicted.	
	during the convective drying	Drying rate increased with	
	of cylindrical	temperature and air	
	quince slices.	velocity.	
	Validated CFD	The model was	Delele et al. (2023)
	model was applied to evaluate the	capable of predicting the	
	performance and	airflow,	
	improve the design	temperature,	
	of a prototype rice	relative humidity	
	husk fuelled mixed	and grain moisture	
	flow rice dryer.	content and it was used to develop	
		better alternative	
		designs and	
Model 1	County of CED DEM	operations.	TT d 1
Multiscale model	Coupled CFD-DEM model was used to	The model was capable of	Handayani et al. (2023)
model	study the drying	predicting the heat	(2020)
	behaviour of	and mass transfer	
	ellipsoidal particles	process, and	
	in fluidized bed dryer, and used to	observed higher drying rate in	
	study the effect of	spherical particles	
	particle aspect	compared to	
	ratio.	ellipsoidal particles	
	2D multiscale water	The multiscale model was capable	Aregawi et al. (2014)
	transport and mechanical model	of predicting the	(2014)
	was applied to	dynamics of the	
	predict water loss	dehydration process	
	and deformation of apple tissue.	and the mechanical deformation at	
	арріс пязие.	different	
		microstructural	
-1 .		compartments.	
Physics informed	A multiscale	This multiscale	Welsh et al. (2021)
hybrid	homogenization model was	model was capable of predicting the	
models	developed on the	diffusivity and gave	
	cellular structure of	a new insight of the	
	apple tissue	homogenization	
	considering intracellular water	approach.	
	and free water		
	separately to		
	calculate the		
	effective diffusivity for convective		
	drying		
	Physics-based and	A reduction of 45 %	Schemminger et al
	Monte Carlo	in drying time and	(2024)
	simulations were	27 % in the required	
	used to predict	energy, and an	
	natural variability	improvement of 8 %	

Table 3 (continued)

Model	Description	Findings	References
Physics informed machine learning model	exposed to hot-air drying process. A physics-informed deep-learning framework capable of encoding the Navier-Stokes equations into the	achieved by increasing the drying air temperature from 50 °C to 70 °C. The applicability of the approach in several physical and medical flow problems was tested	Raissi et al. (2020)
	neural networks was developed A physics-informed Neural Network- based model was implemented to predict moisture concentration and moisture-content- based shrinkage of a plant cell during drying	The approach was capable of predicting moisture concentration and shrinkage, indicating that the approach is a powerful tool for investigating complicated drying mechanisms	Batuwatta-Gamage et al. (2022)

Table 4 Examples of the commonly used empirical drying model equations.

Model	Equation	Reference
Page	$MR = exp(-kt^n)$	Page (1949)
Modified Page	$MR = exp((-kt)^n)$	Yaldiz et al.
Lewis	MR = exp(-kt)	(2001)
	. ,	Lewis (1921)
Henderson and Pabis	MR = aexp(-kt)	Getahun et al. (2021)
Modified Henderson and Pabis	MR = aexp(-kt) + bexp(-gt) + cexp(-ht)	Getahun et al. (2021)
Wang and Singh	$MR = 1 + at + bt^2$	Getahun et al. (2021)
Logarithmic	MR = exp(-kt) + c	Omolola et al. (2014)
Two term exponential	MR = aexp(-kt) + (1-a)exp(-kat)	Yaldiz et al. (2001)
Diffusion approach	MR = aexp(-kt) + (1-a)exp(-kbt)	Getahun et al. (2021)
Verma et al.	MR = aexp(-kt) + (1-a)exp(-gbt)	Verma et al. (1985)
Midilli et al.	$MR = aexp(-kt^n) + bt$	Midilli et al. (2002)

where, MR is the moisture ratio, t is the drying time, k, g, and h are drying constants, n is the order, and a, b, and c are dimensionless constants.

dimensional representations (e.g., NIR spectra, where rows represent samples and columns represent features) to more complex tensor data structures (e.g., hyperspectral images). A common approach to simplify data complexity, especially in hyperspectral imaging, is to fuse spatial information using mean spectra, allowing for a focus on overall quality metrics and system dynamics.

Machine learning models employed in these contexts are generally categorized into static models, which capture spatial dynamics, and time series models, which account for both spatial and temporal patterns. However, most studies continue to employ static machine learning models to estimate the system states (Przybył and Koszela, 2023).

Despite this, static models, such as multilinear regression, support vector machines (SVM), k-nearest neighbors (KNN), and artificial neural networks (ANN), have been effective in identifying key parameters that influence product quality during the drying process (Deng et al., 2010). These methods are often enhanced by preprocessing techniques such as denoising, feature extraction, and feature selection to address the challenges of noisy data and the curse of dimensionality.

A significant advancement in this field is the application of deep learning architectures, particularly Convolutional Neural Networks (CNNs) and hybrid CNN-Long Short-Term Memory (CNN-LSTM) models, which have been successfully applied to monitor spatial foodquality dynamics. CNNs extract and learn spatial features from images, including hyperspectral and RGB images, whereas LSTMs effectively capture temporal trends. The integration of these models has demonstrated promising results, improving both the prediction accuracy and computational efficiency of drying kinetics (George et al., 2022). For instance, the moisture content of potato slices during the drying process was monitored using image chromatic features, with LSTM models achieving higher accuracy, as demonstrated by a Root Mean Square Error (RMSE) of 13×10^{-2} (Sabat et al., 2022). Similarly, Zhou et al. (2022) employed CNN-LSTM to monitor the moisture content in carrot slices using hyperspectral images, achieving high accuracy with an RMSEP of 0.08 %. Other applications of these hybrid models have been demonstrated in the drying of various products such as corn (Simonič and Klančnik, 2024), sweet potatoes (Su et al., 2020), and tea leaves (Xie et al., 2013).

Despite the extensive focus on moisture content, other quality parameters, such as antioxidant retention and vitamin preservation, remain underexplored in studies that incorporate spatial and temporal features. An emerging trend in food drying monitoring is predictive maintenance, in which models are designed to predict product quality and maintain the optimal functioning of the drying equipment. However, the approach of predictive maintenance within the drying process has been the focus of few studies (Rahman et al., 2023). Furthermore, a few studies have investigated monitoring the dynamics of the thermophysical and mechanical properties of products using machine learning (Khan et al., 2022b). This gap in the literature highlights the need for future research to extend machine-learning applications to broader quality metrics during the drying process. Expanding research in this direction could lead to more resilient and adaptable machine-learning models capable of optimizing both product quality and operational efficiency.

Recent literature suggests a growing interest in the generalizability and robustness of machine-learning models across diverse conditions and datasets. Feature selection and model robustness remain key challenges, as variations in raw materials, processing conditions, and sensor data quality can significantly impact the performance of machine learning models in Digital Twins. The future of this research lies in expanding the focus beyond moisture content, enhancing model generalizability in monitoring nutritional components and thermophysical and mechanical properties with spatial and temporal features, and exploring the potential of predictive maintenance in the drying process.

4.1.6. Physics informed machine learning models

Progress in digitalization and advances in sensors and computational and cloud computing resources have created a massive set of data in different applications (Ritto and Rochinha, 2021). The conventional machine-learning approach is one of the most effective data-driven models that has been applied in different applications. However, to obtain an accurate prediction, such conventional machine learning models require a clean dataset as the model input, which means that the raw data should be extracted and processed before it is fed to the model. A data-driven model recommended for automatic real-time raw data processing is a deep learning neural network model (Alzubaidi et al., 2021). Such a model has gained more attention in the drying processes

(Fabani et al., 2021; Martynenko and Misra, 2020; Qadri et al., 2020; Sun et al., 2019a). However, these driven models completely depend on the collected dataset and do not have any physical meaning. Errors during data collection produce inaccurate model predictions (Batuwatta-Gamage et al., 2022; Karniadakis et al., 2021). To increase the accuracy of such data-driven models, there has been a recent development in coupling data-driven models with physics-based models in what is known as Physics-Informed Neural Networks (PINN) (Batuwatta-Gamage et al., 2022; Raissi et al., 2020). The residual losses from the physics-based models were coupled with the losses from the machine learning models through the loss function. The iterative process continues until the loss function satisfies convergence criteria. Studies on the application of PINN in drying are limited (Khan et al., 2020) and further research is required to narrow this knowledge gap. To narrow this knowledge gap, more research on the development and application of a physics-informed machine-learning model is recommended. Such coupled models could help us gain insight into the complex drying process and obtain more accurate predictions of the drying process for optimizing the design, operation, and control of the dryer and troubleshooting.

Mathematical models are capable of predicting the dynamic behavior the drying process, including quality attributes. Furthermore, the models could be timely updated with the real-time data to adapt themselves to the current state of dynamic changes. However, there is still a need to compute the optimal drying trajectories. To this end, the following section presents the dynamic optimization that could be used to compute the optimal drying trajectories. It is followed by subsection 4.2.2 on advanced control required to apply such optimal trajectories.

4.2. Dynamic optimization and advanced control

4.2.1. Dynamic optimization

The problem of Dynamic Optimization (DO), also known as Optimal Control (OC), involves finding the time profile of the control/decision variables (u(t)) that minimize (or maximize) a function representing a performance index of the process. Such an index, defined by the plant operator according to the company's goals, should consider all the relevant product and/or process variables. For instance, the process operator may aim to maximize product quality, minimize process time, energy/resource consumption, or a combination of several factors. Control variables can be manipulated in the process to achieve the desired results. Typical examples in a drying process include inlet air temperature, air flow rate, and humidity of the drying agent. The variables that define the performance of a process are usually related to the state (x(t)). In addition, bounds on the decision variables and constraints of the state variables may be considered. Some examples of constraints during the drying process might be that the drying temperature cannot exceed the capacity of the heating system, the solution found must fulfill the model equations, and/or the product humidity at the end of the process must be below a predefined value. Mathematically, the DO problem can be expressed as:

$$\min_{u(t)} J(x(t), u(t)); \quad \text{with} \quad J(x, u) = f(x(t_f)) + \int_{t_0}^{t_f} g(x(t), u(t)) dt$$

Subject to:

- The model equations (please refer to Section 4.1)
- Algebraic constraints. Equality and inequality constraints can be considered:

$$p(x(t), u(t)) = 0$$

$$q(\mathbf{x}(t), u(t)) \le 0 \tag{3}$$

• Bounds on the control variables

$$\mathbf{x}^L \leq \mathbf{x}(t) \leq \mathbf{x}^U$$

$$u^L < u(t) < u^U \tag{5}$$

The functions $f(x(t_f))$ and g(x(t), u(t)) are defined according to the criteria used to characterize the performance index.

For illustrative purposes, let us consider a particular drying case in which the aim is to determine the time profile of the drying temperature (T(t)) that minimizes the browning of the product at the end of the process $(B(t_f))$ while maintaining the product moisture content at the end of the process $(M(t_f))$ below 14 %. In addition, the drying temperature must be maintained between 40° and 80° °C. The DO problem can be formulated as

$$\min_{T(t)} B(t_f) \tag{6}$$

Subject to:

• The model equations (Kaymak-Ertekin and Gedik, 2005):

$$\frac{\mathrm{d}B}{\mathrm{d}t} = k_0 \, \exp\left(-\frac{E_a}{RT}\right)$$

with initial conditions $B(t=0) = B_0$, $M(t=0) = M_0$, and:

$$k_0 = c_1 M(t)^{c_2}; \quad E_a = c_3 + c_4 M(t)$$
 8

• Algebraic constraints on the moisture content

$$M(t_f) \le 14\%$$

Bounds on the control variable

$$40 \,^{\circ}\text{C} \le T(t) \le 80 \,^{\circ}\text{C}$$

Several methods exist for solving DO problems (Eqs. (1)–(5)). Banga et al. (2005) reviewed the different methods available to address this issue. Typically, these methods are classified into three groups.

- Dynamic Programming (DP) (Grüne, 2019). The DO problem (possibly infinite dimensional) is split into auxiliary problems, which include information about the future of optimal trajectories and where the time horizons are shorter. Although the exact solution is characterized by this approach, the number of auxiliary optimization problems may be large, and their formulation is generally involved.
- Indirect methods (Biegler, 2010). In this approach, the DO problem is transformed into a two-point boundary-value problem using Pontryagin conditions. However, the resulting problem can be solved, as in the previous case. This is particularly true if the state constraints are considered.
- Direct methods (Balsa Canto et al., 2002; Kameswaran and Biegler, 2006). The DO problem is transformed into a non-linear programming problem by discretizing time and approximating either (i) both control and state variables or (ii) only the control variables using particular basis functions (for instance, low-order polynomials). The former approach is known as complete parameterization (CP), whereas the latter is known as control vector parameterization (CVP). The CP approach typically results in a large-scale NLP. However, as shown in (Biegler, 2010), the problem structure and sparsity can be exploited to develop efficient strategies that can maintain a reasonable computational effort.

Table 5 presents the main features of the different studies found in the literature dealing with the DO problem in the context of food drying, particularly for fruits and vegetables. Note that there exist general works that do not focus on food products, whose results can be applied to food matrices. For instance, Kowalski et al. (2013) presented an approach for

Table 5Main features of the different approaches found in the literature to deal with the dynamic optimization problem in the context of fruits and vegetables drying.

Objectives	Control var.	Constraints	Material	Approach	Reference
$Q_p(t_f)$: First order kinetics	$T_{air}^{in}; X_w^{da}$	$X_w^p(t_f); T_p(t_f)$	Granular bioproduct	Not specified	Kamiński (1992)
$N(t_f); t_f;$ E_c	T_{air}^{in}	$X_w^p(t_f); N(t_f);$ $T_p(t)$	Thin slab of cellulose	Indirect method	Banga and Singh (1994)
$N(t_f); E(t_f)$	T_{air}^{in}	$X_w^p(t_f); T_{air}^{in}$	Broccoli	Not specified	Jin et al. (2014a)
$Q_p(t_f)$: Second order kinetics	$T_{air}^{in}; \ X_w^{da}; t_f$	$X_w^p(t_f)$	Rice	Direct (CVP)	Wongrat et al. (2011)
Drying process cost	T_{air}^{in}	$X_w^p(t_f);$ $W_m(t_f); T_{air}^{in}$	Corn	Direct (CVP)	Trelea et al. (1997)
$Q_p(t_f)$: Second order kinetics	T_{air}^{in},X_{w}^{da}	$X_w^p\left(t_f ight)$	Rice	Direct (CVP)	Olmos et al. (2002)
t_f	T_{air}^{in}	$X_w^p(t_f);$ $W_m(t_f)$	Corn	Direct (CVP)	TRELEA et al. (1999)
$Q_p(t_f)$: first order kinetics	$T_{air}^{in};F^{da}$	$X_w^p(t_f); T_{air}^{in};$ F^{da}	Broccoli	Direct (CVP)	Jin et al. (2014b)

DO in the drying of porous materials, which is typical in food matrices; Barttfeld et al. (2006) dealt with the DO problem of multiple-zone air impingement driers for drying thin liquid films on continuous substrates. However, these studies were not included in this review. As listed in Table 1, the inlet air temperature (T_{air}^{in}) was the main control variable. The humidity of the drying agent (X_w^{da}), drying agent flow rate (F^{da}) , and drying time (t_f) have also been considered. The drying agent was air. Regarding the selection of the objective function to be optimized in the DO problem, the preferred option is to maximize the product quality at the end of the process $(Q_p(t_f))$, which is equivalent to minimizing quality degradation. Typically, studies have focused on a general quality concept described by first- or second-order kinetics, although some studies have considered a particular quality indicator, such as nutrients $(N(t_f))$ or enzymes $(E(t_f))$. The minimization of energy consumption (E_c) , process cost (C_p) , and drying time are also objectives considered in the literature. The most widely considered constraint is the moisture content in the product at the end of the process $(X_w^p(t_f))$. Other constraints considered in the literature are the product temperature, both during the process $(T_p(t))$ and at the end of the process $(T_p(t_f))$, and the wet-milling quality $(W_m(t_f))$. Finally, as shown in Table 5, the CVP method was the preferred approach for solving the DO problem in the context of fruit and vegetable drying.

4.2.2. Advanced control

The approach described in the previous section allows the computation of drying policies that result in the optimization of one or several relevant variables (product quality, energy consumption, process time, etc.). However, as the reader might notice, there was no feedback from the plant. Therefore, in DO, issues such as plant-model mismatch, unmeasured process disturbances, and differences between the optimal control obtained and the implemented control, among others, have an impact on the process that cannot be corrected online. Therefore, the control scheme must consider the feedback from the plant. PID

controllers are the most typical type of controller used in the drying process. Although, in general, PID provide good results, the combination of plant information and mathematical models allow for different control schemes that can improve the performance of PID controllers has been studied in the last decades. Note that a mathematical model allows us to predict the evolution of different variables and react beforehand.

One of the main advanced control strategies used in the context of the drying process is Model Predictive Control (MPC) (García et al., 1989). The problem to be solved is the DO problem, as discussed in the previous section. Time discretization and approximation of the control variables using low-order polynomials were also used in the MPC. However, in the case of MPC, the DO problem is solved over a finite horizon, and although different cost functions might be used, they typically consider two terms: (i) a measure of the distance between the state variables and the reference trajectory for such variables, and (ii) a penalty on the control effort. Mathematically, the optimization problem to be solved is as follows:

$$\min_{u(t)} J(x,u); \quad \text{with} \quad J(x,u) = \sum_{i=1}^{N} \left[\left(x(t_{k+i}) - x^{ref}(t_{k+i}) \right)^2 + \omega_i \Delta u(t_{k+i})^2 \right]$$

Subject, as in the previous section, to constraints such as the model equations, bounds on the decision variables, and other constraints on the state variables. In Eq. (11), N is the number of control sequences, k is the current time step, and $x^{ref}(t)$ is the value of the reference trajectory. In addition, in contrast to the DO problem, the MPC strategy receives feedback from the system. Only the first step of control discretization is applied to the system from the optimal profile obtained after solving the DO problem. At the end of that step, the state of the process is measured, this information is used to compute a new profile of the control variables, and the procedure is repeated.

Regarding the application of MPC to the drying process, Han et al. (2012) developed an MPC strategy based on neural networks for drying grains. The authors also used the PDE model to describe the drying process. The controller improved the uniformity of the moisture content, ensuring grain quality. More recently, an MPC strategy for the intermittent drying of paddy rice with the objective of maximizing head rice yield (HRY) was considered (Song et al., 2022). The idea was to use the adjusted evaluation index of the predicted HRY as the performance index to calculate the optimal control trajectories in real-time. Arun Jayakar et al. (2021) developed a mathematical model for a hot-air generator using a transfer function model. The authors also developed PID and MPC strategies to control the drying of tea leaves based on this model. Disturbances in environmental temperature and blower speed were considered. The exact transfer function model was obtained by conducting open-loop tests. The model was fine-tuned, and integer and non-integer models were obtained using different optimization techniques. Cristea (2015) developed an MPC strategy to control product temperature and improve the drying process of slab-shaped food products. Ramp-constant temperature setpoints are also considered.

From another point of view, Fuzzy Logic concepts were also used to design efficient controllers for the drying process. Boeri et al. (2013) developed a nonlinear MIMO fuzzy logic controller composed of four fuzzy controllers to track temperature, relative humidity, and air velocity. Their controller showed much better performance than a PID controller. Liu et al. (2006) used the Principal Component Analysis (PCA) concept to design a control strategy for maize drying that can deal with nonlinearity, long delay, and multi-variable issues. In this study, a PCA model was developed. The predicted scores were fed to a predictive model that was developed using the neural network partial least squares. These predicted scores were used as indicators of process performance. Vega et al. (2016) proposed a lumped parameter model based on experimental results for both the drying process of apple slices and the automatic control functionality. The simulation model showed a close correlation with the experimental data and thus could be used to

determine the optimum control and process parameters for the convective drying of apple slices. Application of this strategy led to a significant decrease in drying time and, potentially, an increase in process efficiency and product quality.

5. Future research needs

Digital Twins-based smart food drying is still in its infancy. The literature review is more limited to the development of digital models. Further research is required to develop digital shadows and future Digital Twins. The main reason for postponing the appearance of Digital Twins-based smart food dryers is the interdisciplinary nature of the topic, which requires knowledge from different areas. The current paper aims to provide a better insight into the concept and lightens the way how Digital Twins can be brought into drying technology. To reach this goal, future research should focus on:

- A clearer understanding of the interdependencies between product changes, process settings, and physical setup is required. Based on these new indicators, it may be necessary to make the machine more readable.
- Noninvasive monitoring of chemical compounds needs to be further developed. Even though there is a wealth of studies on the monitoring of moisture content, color, shrinkage, and some other physical attributes, many of the core nutritional components, so far, have not been sufficiently included. Although there have been some studies on pigments and polyphenols, more investigation is needed to extend the monitoring process to include more chemical components, such as vitamins.
- Most previous studies were conducted under static drying conditions, where the drying process was conducted under a constant air temperature, humidity, and velocity. There are few studies on dynamic/variable drying conditions, particularly with respect to the drying process of fruits and vegetables. As in a Digital Twins-based smart food dryer, the strategy is to tune the drying conditions throughout the process, there is still room for the dynamic optimization of the fruit and vegetable drying process.
- Other tools from the Process Engineering field should be integrated into Digital Twins (Prada et al., 2022) of the drying process. In this regard, the development of State Observers that combine mathematical models and plant information to reduce plant-model mismatch and their integration into advanced control schemes must be studied. Fault detection strategies that allow the identification of problems in sensors should be studied and implemented during the drying process. In addition, a Digital Twins-based smart food drying process should also consider Data Reconciliation techniques that allow the consideration and improvement of coherence among measurements and between measurements and model predictions, compute key performance indexes, or estimate unknown magnitudes. Finally, a Digital Twins-based smart food drying process should include a database capable of managing large quantities of data and Big Data analysis tools that allow for easy and fast interpretation of such data.
- The concept presented in this study is based on the hybrid application of data-driven and mathematical models. First, real-time data collected by the sensors are fed to data-driven models to estimate the quality attributes. Next, those estimations are fed to the mathematical models. Subsequently, dynamic optimization compute the optimal trajectories. Finally, the optimal trajectories are fed back to an advanced control unit. Currently, given the rapid growth of machine learning algorithms and their huge potential to learn deeply from data, it is a potential research topic to leave everything to machine learning algorithms. In other words, the machine learning algorithms perform both prediction and decision-making tasks. Learning from data could be advantageous over the mathematical

- modeling of the process in which some parameters could be simplified or overlooked.
- Finally, Jones et al. (2020) identified perceived benefits, Digital Twins across the product lifecycle, technical implementations, levels of fidelity, data ownership, and integration between virtual entities as knowledge gaps and topics for future research.

CRediT authorship contribution statement

Arman Arefi: Conceptualization, Writing – original draft, Writing – review & editing. Carlos Vilas: Writing – original draft, Writing – review & editing. Mulugeta Admasu Delele: Writing – original draft, Writing – review & editing. Petra Foerst: Writing – original draft, Writing – review & editing. Sebastian Gruber: Writing – original draft, Writing – review & editing. Mohammad Kaveh: Writing – original draft. Farhad Khoshnam: Writing – original draft. Norhashila Hashim: Writing – original draft. Maimunah Mohd Ali: Writing – original draft. Saman Zohrabi: Writing – original draft, Muhammad Tayyab: Writing – original draft. Aditya Parmar: Writing – original draft. Pramod Aradwad: Writing – original draft. John Ndisya: Writing – original draft. Waseem Amjad: Writing – original draft. Majharulislam Babor: Writing – original draft Annika Mahn: Coordination, Writing – review & editing. Barbara Sturm: Conceptualization, Writing – original draft, Writing – review & editing.

Declaration of generative AI and AI-assisted technologies in the writing process

During the preparation of this work, the author(s) used ChatGPT (by OpenAI) in order to improve the readability and language of the manuscript. After using this tool/service, the author(s) reviewed and edited the content as needed and take(s) full responsibility for the content of the published article.

Declaration of competing interest

The authors declare that they have no known competing financial interests or personal relationships that could have appeared to influence the work reported in this paper.

Acknowledgment

We would like to thank Leibniz Institute for Agricultural Engineering and Bioeconomy (ATB) for the financial support of this study. Special thanks are extended to Dr. Thomas Hoffmann, Head of the Systems Process Engineering Department, for his support and guidance.

Data availability

No data was used for the research described in the article.

References

- Abouelenein, D., Mustafa, A.M., Angeloni, S., Borsetta, G., Vittori, S., Maggi, F., Sagratini, G., Caprioli, G., 2021. Influence of freezing and different drying methods on volatile profiles of strawberry and analysis of volatile compounds of strawberry commercial jams. Molecules 26, 4153.
- Aktaş, M., Sözen, A., Amini, A., Khanlari, A., 2017. Experimental analysis and CFD simulation of infrared apricot dryer with heat recovery. Dry. Technol. 35, 766–783. https://doi.org/10.1080/07373937.2016.1212871.
- Albanese, D., Cinquanta, L., Cuccurullo, G., Di Matteo, M., 2013. Effects of microwave and hot-air drying methods on colour, β-carotene and radical scavenging activity of apricots. Int. J. Food Sci. Technol. 48, 1327–1333.
- Allgöwer, F., Badgwell, T.A., Qin, J.S., Rawlings, J.B., Wright, S.J., 1999. Nonlinear predictive control and moving horizon estimation—an introductory overview. Advances in control: Highlights of ECC' 99, 391–449.
- Alonzo-Macías, M., Montejano-Gaitán, G., Allaf, K., 2014. Impact of drying processes on strawberry (Fragaria var. C amarosa) texture: identification of crispy and crunchy features by instrumental measurement. J. Texture Stud. 45, 246–259. https://doi. org/10.1111/jtxs.12070.

- Alzubaidi, L., Zhang, J., Humaidi, A.J., Al-Dujaili, A., Duan, Y., Al-Shamma, O., Santamaría, J., Fadhel, M.A., Al-Amidie, M., Farhan, L., 2021. Review of deep learning: concepts, CNN architectures, challenges, applications, future directions. Journal of big data 8, 1–74. am Goula, Adamopoulos, KG, 2006. Retention of ascorbic acid during drying of tomato halves and tomato pulp. Dry. Technol. 24, 57–64.
- Antal, T., Kerekes, B., Sikolya, L., Tarek, M., 2015. Quality and drying characteristics of apple cubes subjected to combined drying (FD pre-drying and HAD finish-drying). J. Food Process. Preserv. 39, 994–1005. https://doi.org/10.1111/jfpp.12313.
- Aradwad, P.P., Thirumani Venkatesh, A.K., Mani, I., 2023. Infrared drying of apple (Malus domestica) slices: effect on drying and color kinetics, texture, rehydration, and microstructure. J. Food Process. Eng. 46, e14218.
- Aral, S., Beşe, A.V., 2016. Convective drying of hawthorn fruit (Crataegus spp.): effect of experimental parameters on drying kinetics, color, shrinkage, and rehydration capacity. Food Chem. 210, 577–584.
- Arefi, A., Sturm, B., Gersdorff, G. von, Nasirahmadi, A., Hensel, O., 2021. Vis-NIR hyperspectral imaging along with Gaussian process regression to monitor quality attributes of apple slices during drying. LWT 152, 112297. https://doi.org/10.1016/ i.lwt.2021.112297.
- Arefi, A., Sturm, B., Hensel, O., Raut, S., 2023a. NIR monochrome imaging for monitoring of apple drying process: light-emitting diode and Band-pass filter imaging techniques. Food Biosci. 54, 102898. https://doi.org/10.1016/j. fbio.2023.102898.
- Arefi, A., Sturm, B., Raut, S., Gersdorff, G. von, Hensel, O., 2023b. NIR laser-based imaging techniques to monitor quality attributes of apple slices during the drying process: laser-light backscattering & biospeckle imaging techniques. Food Control 143, 109289.
- Aregawi, W.A., Abera, M.K., Fanta, S.W., Verboven, P., Nicolai, B., 2014. Prediction of water loss and viscoelastic deformation of apple tissue using a multiscale model. J. Phys. Condens. Matter 26, 464111.
- Arun Jayakar, S., Tamilselvan, G.M., Sundararajan, T.V.P., Rajesh, T., 2021. An investigation on hybrid optimization-based proportional integral derivative and model predictive controllers for three tank interacting system. In: Pandian, A.P., Palanisamy, R., Ntalianis, K. (Eds.), Proceedings of International Conference on Intelligent Computing, Information and Control Systems, vol 1272. Springer, Singapore, Singapore, pp. 125–145.
- Asemu, A.M., Habtu, N.G., Delele, M.A., Subramanyam, B., Alavi, S., 2020. Drying characteristics of maize grain in solar bubble dryer. J. Food Process. Eng. 43, e13312.
- Bai, J.-W., Zhang, L., Cai, J.-R., Wang, Y.-C., Tian, X.-Y., 2021. Laser light backscattering image to predict moisture content of mango slices with different ripeness during drying process. J. Food Process. Eng. 44, e13900. https://doi.org/10.1111/ ifpe.13900.
- Balsa Canto, E., Banga, J.R., Alonso, A.A., Vassiliadis, V.S., 2002. Restricted second order information for the solution of optimal control problems using control vector parameterization. J. Process Control 12, 243–255. https://doi.org/10.1016/S0959-1524(01)00008-7.
- Balzarini, M.F., Reinheimer, M.A., Ciappini, M.C., Scenna, N.J., 2018. Comparative study of hot air and vacuum drying on the drying kinetics and physicochemical properties of chicory roots. J. Food Sci. Technol. 55, 4067–4078.
- Banga, J.R., Balsa-Canto, E., Moles, C.G., Alonso, A.A., 2005. Dynamic optimization of bioprocesses: efficient and robust numerical strategies. J. Biotechnol. 117, 407–419.
- Banga, J.R., Singh, R.P., 1994. Optimization of air drying of foods. J. Food Eng. 23, 189–211.
- Barbieri, S., Elustondo, M., Urbicain, M., 2004. Retention of aroma compounds in basil dried with low pressure superheated steam. J. Food Eng. 65, 109–115.
- Barttfeld, M., Alleborn, N., Durst, F., 2006. Dynamic optimization of multiple-zone air impingement drying processes. Comput. Chem. Eng. 30, 467–489.
- Batuwatta-Gamage, C.P., Rathnayaka, C.M., Karunasena, H.C.P., Wijerathne, W., Jeong, H., Welsh, Z.G., Karim, M.A., Gu, Y.T., 2022. A physics-informed neural network-based surrogate framework to predict moisture concentration and shrinkage of a plant cell during drying. J. Food Eng. 332, 111137.
- Beigi, M., 2017. Thin layer drying of wormwood (Artemisia absinthium L.) leaves: dehydration characteristics, rehydration capacity and energy consumption. Heat Mass Tran. 53, 2711–2718.
- Beigi, M., 2019. Drying of mint leaves: influence of the process temperature on dehydration parameters, quality attributes, and energy consumption. J. Agric. Sci. Technol. 21, 77–88.
- Biegler, L.T., 2010. Nonlinear Programming: Concepts, Algorithms, and Applications to Chemical Processes. SIAM.
- Boeri, C.N., Da Silva, F.N., Ferreira, J., 2013. High performance controller for drying processes. Acta Sci. Technol. 35. https://doi.org/10.4025/actascitechnol. v35i2.14775.
- Bogale Teseme, W., Weldemichael Weldeselassie, H., 2020. Review on the study of dielectric properties of food materials. American Journal of Engineering and Technology Management 5, 76. https://doi.org/10.11648/j.ajetm.20200505.11.
- Bombana, V.B., Fischer, B., Oro, C.E.D., Rigo, D., Polina, C.C., Franco Denti, A., Gonçalves, T.d.S., Steffens, C., Cansian, R.L., Toniazzo Backes, G., 2023. Drying kinetics of guabiju pulp (Myrcianthes pungens): mass transfer parameters, mathematical modeling and evaluation of bioactive compounds. J. Food Process. Eng. 46, e14205.
- Borovkova, M., Khodzitsky, M., Demchenko, P., Cherkasova, O., Popov, A., Meglinski, I., 2018. Terahertz time-domain spectroscopy for non-invasive assessment of water content in biological samples. Biomed. Opt. Express 9, 2266–2276. https://doi.org/ 10.1364/BOE.9.002266.

- Boudhrioua, N., Giampaoli, P., Bonazzi, C., 2003. Changes in aromatic components of banana during ripening and air-drying. LWT 36, 633–642.
- Braeuer, A.S., Schuster, J.J., Gebrekidan, M.T., Bahr, L., Michelino, F., Zambon, A., Spilimbergo, S., 2017. In situ Raman analysis of CO₂-assisted drying of fruit-slices. Foods 6. https://doi.org/10.3390/foods6050037.
- Brown, Z.K., Fryer, P.J., Norton, I.T., Bakalis, S., Bridson, R.H., 2008. Drying of foods using supercritical carbon dioxide investigations with carrot. Innov. Food Sci. Emerg. Technol. 9, 280–289. https://doi.org/10.1016/j.ifset.2007.07.003.
- Carvalho, D.G., Sebben, J.A., Moura, N.F. de, Trierweiler, J.O., Da Espindola, J.S., 2019. Raman spectroscopy for monitoring carotenoids in processed Bunchosia glandulifera pulps. Food Chem. 294, 565–571. https://doi.org/10.1016/j. foodchem.2019.04.120.
- Castro, A.M., Díaz, L.E., Quintanilla-Carvajal, M.X., Mayorga, E.Y., Moreno, F.L., 2023. Convective drying of feijoa (Acca sellowiana Berg): a study on bioactivity, quality, and drying parameters. LWT 186, 115209.
- Chakravartula, S.S.N., Bandiera, A., Nardella, M., Bedini, G., Ibba, P., Massantini, R., Moscetti, R., 2023. Computer vision-based smart monitoring and control system for food drying: a study on carrot slices. Comput. Electron. Agric. 206, 107654.
- Chandramohan, V.P., 2016. Experimental analysis and simultaneous heat and moisture transfer with coupled CFD model for convective drying of moist object. Int. J. Comput. Methods Eng. Sci. Mech. 17, 59–71.
- Chao, E., Li, J., Fan, L., 2022. Enhancing drying efficiency and quality of seed-used pumpkin using ultrasound, freeze-thawing and blanching pretreatments. Food Chem. 384, 132496. https://doi.org/10.1016/j.foodchem.2022.132496.
- Chayjan, R.A., Salari, K., Shadidi, B., 2012. Modeling Some Drying Characteristics of Garlic Sheets Under Semi Fluidized and Fluidized Bed Conditions.
- Chen, C., Venkitasamy, C., Zhang, W., Deng, L., Meng, X., Pan, Z., 2020a. Effect of step-down temperature drying on energy consumption and product quality of walnuts. J. Food Eng. 285, 110105. https://doi.org/10.1016/j.jfoodeng.2020.110105.
- Chen, X., Jiao, Y., Liu, B., Chao, W., Duan, X., Yue, T., 2022. Using hyperspectral imaging technology for assessing internal quality parameters of persimmon fruits during the drying process. Food Chem. 386, 132774.
- Chen, X.D., Pirini, W., Ozilgen, M., 2001. The reaction engineering approach to modeling drying of thin layer of pulped Kiwifruit flesh under conditions of small Biot numbers. Chem. Eng. Process. Process Intensif. 40, 311–320.
- Chen, Y., Li, M., Dharmasiri, T.S.K., Song, X., Liu, F., Wang, X., 2020b. Novel ultrasonic-assisted vacuum drying technique for dehydrating garlic slices and predicting the quality properties by low field nuclear magnetic resonance. Food Chem. 306, 125625. https://doi.org/10.1016/j.foodchem.2019.125625.
- Chikpah, S.K., Korese, J.K., Sturm, B., Hensel, O., 2022. Colour change kinetics of pumpkin (Cucurbita moschata) slices during convective air drying and bioactive compounds of the dried products. J. Agric. Food Res. 10, 100409.
- Chitrakar, B., Zhang, M., Bhandari, B., 2019. Novel intelligent detection of safer water activity by LF-NMR spectra for selected fruits and vegetables during drying. Food Bioprocess Technol. 12, 1093–1101. https://doi.org/10.1007/s11947-019-02278-y.
- Chitrakar, B., Zhang, M., Zhang, X., 2021. The determination of drying end-point for asparagus by-products with the use of LF-NMR spectra. Dry. Technol. 39, 1158–1164. https://doi.org/10.1080/07373937.2020.1766484.
- Cristea, V.M., 2015. Model predictive control of the temperature in drying food products. Studia Universitatis Babes-Bolyai. Chemia 60, 157–164.
- Da Cruz, P.M., Braga, G.C., de Grandi, am, 2012. Chemical Composition, Color and Sensory Quality of Tomato Dried at Different Temperatures.
- Da Silva, F.R.G.B., Souza, M. de, Da Costa, A.M.d.S., Matos Jorge, L.M. de, Paraíso, P.R., 2012. Experimental and numerical analysis of soybean meal drying in fluidized bed. Powder Technol. 229, 61–70.
- Darvishi, H., Khodaie, J., Azadbakht, M., 2015. The parameters of mass transfer of convective drying in sliced melon. Philippine Agric. Sci. 98, 60–72.
- Datta, A.K., 2016. Toward computer-aided food engineering: mechanistic frameworks for evolution of product, quality and safety during processing. J. Food Eng. 176, 9–27.
- Defraeye, T., 2014. Advanced computational modelling for drying processes-A review. Appl. Energy 131, 323–344.
- Del Razola-Díaz, M.C., Verardo, V., Gómez-Caravaca, A.M., García-Villanova, B., Guerra-Hernández, E.J., 2023. Mathematical modelling of convective drying of orange by-product and its influence on phenolic compounds and ascorbic acid content, and its antioxidant activity. Foods 12, 500.
- Delele, M.A., Mihret, Y.C., Mellmann, J., 2023. Performance evaluation and improvement of prototype rice husk fueled mixed flow rough rice dryer using CFD model. Dry. Technol. 41, 2447–2463. https://doi.org/10.1080/ 07373937.2023.2252056.
- Demiray, E., Tulek, Y., Yilmaz, Y., 2013. Degradation kinetics of lycopene, β-carotene and ascorbic acid in tomatoes during hot air drying. LWT 50, 172–176. https://doi.org/10.1016/j.lwt.2012.06.001.
- Demiray, E., Yazar, J.G., Aktok, Ö., Çulluk, B., Çalışkan Koç, G., Pandiselvam, R., 2023. The effect of drying temperature and thickness on the drying kinetic, antioxidant activity, phenolic compounds, and color values of apple slices. J. Food Qual. 2023, 1-12
- Deng, M., Wen, S., Yanou, A., Oka, M., Matsumoto, H., Inoue, A., 2010. SVM-based moisture content modelling for Sugi drying process. In: Proceedings of the 2010 International Conference on Modelling, Identification and Control. IEEE, pp. 354–358.
- Di Scala, K., Vega-Gálvez, A., Uribe, E., Oyanadel, R., Miranda, M., Vergara, J., Quispe, I., Lemus-Mondaca, R., 2011. Changes of quality characteristics of pepino fruit (Solanum muricatum ait) during convective drying. Int. J. Food Sci. Technol. 46, 746–753. https://doi.org/10.1111/j.1365-2621.2011.02555.x.
- Ek, P., Araújo, A.C., Oliveira, S.M., Ramos, I.N., Brandão, T.R.S., Silva, C.L.M., 2018. Assessment of nutritional quality and color parameters of convective dried

- watercress (Nasturtium officinale). J. Food Process. Preserv. 42, e13459. https://doi.org/10.1111/ifpp.13459.
- Fabani, M.P., Capossio, J.P., Román, M.C., Zhu, W., Rodriguez, R., Mazza, G., 2021. Producing non-traditional flour from watermelon rind pomace: artificial neural network (ANN) modeling of the drying process. J. Environ. Manag. 281, 111915.
- Farias, R.P., Gomez, R.S., Silva, W.P., Silva, L.P.L., Oliveira Neto, G.L., Santos, I.B., Carmo, J.E.F., Nascimento, J.J.S., Lima, A.G.B., 2020. Heat and mass transfer, and volume variations in banana slices during convective hot air drying: an experimental analysis. Agriculture 10, 423.
- Foerst, P., Melo de Carvalho, T., Lechner, M., Kovacevic, T., Kim, S., Kirse, C., Briesen, H., 2019. Estimation of mass transfer rate and primary drying times during freeze-drying of frozen maltodextrin solutions based on x-ray μ -computed tomography measurements of pore size distributions. J. Food Eng. 260, 50–57. https://doi.org/10.1016/j.jfoodeng.2019.05.002.
- Fulladosa, E., Rubio-Celorio, M., Skytte, J.L., Muñoz, I., Picouet, P., 2017. Laser-light backscattering response to water content and proteolysis in dry-cured ham. Food Control 77, 235–242.
- García, C.E., Prett, D.M., Morari, M., 1989. Model predictive control: theory and practice—A survey. Automatica 25, 335–348. https://doi.org/10.1016/0005-1098 (89)90002-2
- Ge, S., Chen, Y., Ding, S., Zhou, H., Jiang, L., Yi, Y., Deng, F., Wang, R., 2020. Changes in volatile flavor compounds of peppers during hot air drying process based on headspace-gas chromatography-ion mobility spectrometry (HS-GC-IMS). J. Sci. Food Agric. 100, 3087–3098. https://doi.org/10.1002/jsfa.10341.
- George, O.A., Putranto, A., Xiao, J., Olayiwola, P.S., Chen, X.D., Ogbemhe, J., Akinyemi, T.J., Kharaghani, A., 2022. Deep neural network for generalizing and forecasting on-demand drying kinetics of droplet solutions. Powder Technol. 403, 117392. https://doi.org/10.1016/j.powtec.2022.117392.
 Getahun, E., Gabbiye, N., Delele, M.A., Fanta, S.W., Vanierschot, M., 2021. Two-stage
- Getahun, E., Gabbiye, N., Delele, M.A., Fanta, S.W., Vanierschot, M., 2021. Two-stage solar tunnel chili drying: drying characteristics, performance, product quality, and carbon footprint analysis. Sol. Energy 230, 73–90.
- Ghosh, D., Datta, A., 2023. Deep learning enabled surrogate model of complex food processes for rapid prediction. Chem. Eng. Sci. 270, 118515. https://doi.org/ 10.1016/j.ces.2023.118515.
- Goli, H., Ghamari, S., Khanahmadzadeh, A., 2023. Drying kinetics, modeling and quality of quince slices in thin layer air impingement jet dryer. Agric. Eng. Int. CIGR J. 25.
- Gong, C., Liao, M., Zhang, H., Xu, Y., Miao, Y., Jiao, S., 2020. Investigation of hot air–assisted radio frequency as a final-stage drying of pre-dried carrot cubes. Food Bioprocess Technol. 13, 419–429. https://doi.org/10.1007/s11947-019-02400-0.
- Gong, Z., Di, Deng, Sun, X., Liu, J., Ouyang, Y., 2022. Non-destructive detection of moisture content for Ginkgo biloba fruit with terahertz spectrum and image: a preliminary study. Infrared Phys. Technol. 120, 103997. https://doi.org/10.1016/j. infrared.2021.103997.
- Gruber, S., Vorhauer-Huget, N., Foerst, P., 2021. In situ micro-computed tomography to study microstructure and sublimation front during freeze-drying. Food Struct. 29, 100213. https://doi.org/10.1016/j.foostr.2021.100213.
- Grüne, L., 2019. Dynamic programming, optimal control and model predictive control. In: Raković, S.V., Levine, W.S. (Eds.), Handbook of Model Predictive Control. Springer International Publishing, Cham, pp. 29–52.
- Guiné, R.P.F., Barroca, M.J., Gonçalves, F.J., Alves, M., Oliveira, S., Correia, P., 2015. Effect of drying on total phenolic compounds, antioxidant activity, and kinetics decay in pears. Int. J. Fruit Sci. 15, 173–186.
- Guo, H.-L., Chen, Y., Xu, W., Xu, M.-T., Sun, Y., Wang, X.-C., Wang, X.-Y., Luo, J., Zhang, H., Xiong, Y.-K., 2022. Assessment of drying kinetics, textural and aroma attributes of mentha haplocalyx leaves during the hot air thin-layer drying process. Foods 11, 784
- Han, F., Zuo, C., Wu, W., Li, J., Liu, Z., 2012. Model predictive control of the grain drying process. Math. Probl Eng. 2012, 584376. https://doi.org/10.1155/2012/584376.
- Handayani, S.U., Wahyudi, H., Agustina, S., Yulianto, M.E., Ariyanto, H.D., 2023. CFD-DEM study of heat and mass transfer of ellipsoidal particles in fluidized bed dryers. Powder Technol. 425, 118535.
- Hausman, D.S., Cambron, R.T., Sakr, A., 2005. Application of on-line Raman spectroscopy for characterizing relationships between drug hydration state and tablet physical stability. Int. J. Pharm. 299, 19–33.
- Ho, Q.T., Verboven, P., Verlinden, B.E., Herremans, E., Wevers, M., Carmeliet, J., Nicolaï, B.M., 2011. A three-dimensional multiscale model for gas exchange in fruit. Plant Physiol. 155, 1158–1168.
- Hou, Z., Wei, Y., Sun, L., Xia, R., Xu, H., Li, Y., Feng, Y., Fan, W., Xin, G., 2022. Effects of drying temperature on umami taste and aroma profiles of mushrooms (Suillus granulatus). J. Food Sci. 87, 1983–1998. https://doi.org/10.1111/1750-3841.16127.
- Huang, L.-L., Lian, M.-M., Duan, X., Li, B., Yang, S.-Z., 2021. Studies on the quality and moisture distribution of kiwifruit dried by freeze drying combined with microwave vacuum drying. J. Food Process. Eng. 44. https://doi.org/10.1111/jfpe.13581.
- Huang, W., Huang, D., Qin, Y., Zhang, Y., Lu, Y., Huang, S., Gong, G., 2023. Ultrasound-assisted hot air drying characteristics of Phyllanthus emblica. J. Food Process. Eng. 46, e14286.
- Iheonye, A., Gariepy, Y., Raghavan, V., 2020. Computer vision for real-time monitoring of shrinkage for peas dried in a fluidized bed dryer. Dry. Technol. 38, 130–146. https://doi.org/10.1080/07373937.2019.1649277.
- Islam, M.Z., Saha, T., Monalisa, K., Hoque, M.M., 2019. Effect of starch edible coating on drying characteristics and antioxidant properties of papaya. Food Measure 13, 2951–2960.
- Izli, N., Izli, G., Taskin, O., 2017. Drying kinetics, colour, total phenolic content and antioxidant capacity properties of kiwi dried by different methods. Food Measure 11, 64–74.

- Izli, N., Polat, A., 2019. Freeze and convective drying of quince (Cydonia oblonga Miller.): effects on drying kinetics and quality attributes. Heat Mass Tran. 55, 1317–1326.
- Javanbakht, N., Xiao, G., Amaya, R.E., 2021a. A comprehensive review of portable microwave sensors for grains and mineral materials moisture content monitoring. IEEE Access 9, 120176–120184. https://doi.org/10.1109/ACCESS.2021.3108906.
- Javanbakht, N., Xiao, G., Amaya, R.E., Sangha, J., Ruan, Y., 2021b. Compact frequency selective surface antenna for grain moisture content monitoring. In: 2021 IEEE 19th International Symposium on Antenna Technology and Applied Electromagnetics (ANTEM), Winnipeg, MB, Canada. 8/8/2021 - 8/11/2021. IEEE, pp. 1–2.
- Jiang, Y., Jin, X., Xu, F., Chen, X.D., 2019. Quantifying food drying rates from NMR/MRI experiments: development of an online calibration system. Dry. Technol. 37, 2047–2058. https://doi.org/10.1080/07373937.2018.1552291.
- Jin, X., Oliviero, T., van der Sman, R.G., Verkerk, R., Dekker, M., van Boxtel, A.J., 2014a. Impact of different drying trajectories on degradation of nutritional compounds in broccoli (Brassica oleracea var. italica). LWT 59, 189–195.
- Jin, X., van der Sman, R., van Straten, G., Boom, R.M., van Boxtel, A., 2014b. Energy efficient drying strategies to retain nutritional components in broccoli (Brassica oleracea var. italica). J. Food Eng. 123, 172–178. https://doi.org/10.1016/j. jfoodeng.2013.09.016.
- Jödicke, K., Zirkler, R., Eckhard, T., Hofacker, W., Jödicke, B., 2020. High end quality measuring in mango drying through multi-spectral imaging systems. ChemEngineering 4, 8.
- Jones, D., Snider, C., Nassehi, A., Yon, J., Hicks, B., 2020. Characterising the digital twin: a systematic literature review. CIRP J. Manuf. Sci. Technol. 29, 36–52. https://doi. org/10.1016/j.cirpj.2020.02.002.
- Joshi, A., Rupasinghe, H., Khanizadeh, S., 2011. Impact of drying processes on bioactive phenolics, vitamin c and antioxidant capacity of red-fleshed apple slices. J. Food Process. Preserv. 35, 453–457. https://doi.org/10.1111/J.1745-4549.2010.00487.
- Kalantari, D., Naji-Tabasi, S., Kaveh, M., Azadbakht, M., Majnooni, M., Khorshidi, Y., Asghari, A., Khalife, E., 2023. Drying kinetics and shrinkage rate of thin-sliced pears in different drying stages. J. Food Process. Eng. 46, e14264.
- Kamal, T., Song, Y., Tan, Z., Zhu, B.-W., Tan, M., 2019. Effect of hot-air oven dehydration process on water dynamics and microstructure of apple (Fuji) cultivar slices assessed by LF-NMR and MRI. Dry. Technol. 37, 1974–1987. https://doi.org/10.1080/ 07373937.2018.1547312.
- Kamble, M., Singh, A., Singh, S.V., Chinchkar, A., Pareek, S., 2022. Optimization of convective tray-drying process parameters for green banana slices using response surface methodology and its characterization. J. Food Qual. 2022.
- Kameswaran, S., Biegler, L.T., 2006. Simultaneous dynamic optimization strategies: recent advances and challenges. Comput. Chem. Eng. 30, 1560–1575.
- Kamiński, W., 1992. Optimal control of bioproduct drying with respect to product quality. Chem. Eng. Process. Process Intensif. 31, 125–129.
- Karabulut, I., Topcu, A., Duran, A., Turan, S., Ozturk, B., 2007. Effect of hot air drying and sun drying on color values and β-carotene content of apricot (Prunus armenica L.). LWT 40, 753–758. https://doi.org/10.1016/j.lwt.2006.05.001.
- Karniadakis, G.E., Kevrekidis, I.G., Lu, L., Perdikaris, P., Wang, S., Yang, L., 2021. Physics-informed machine learning. Nature Reviews Physics 3, 422–440.
- Kaur, R., Kaur, K., Ahluwalia, P., 2020. Effect of drying temperatures and storage on chemical and bioactive attributes of dried tomato and sweet pepper. LWT 117, 108604. https://doi.org/10.1016/j.lwt.2019.108604.
- Kaveh, M., Golpour, I., Gonçalves, J.C., Ghafouri, S., Guiné, R., 2021. Determination of drying kinetics, specific energy consumption, shrinkage, and colour properties of pomegranate arils submitted to microwave and convective drying. Open Agric. 6, 230–242.
- Kaya, A., Aydın, O., Kolaylı, S., 2010. Effect of different drying conditions on the vitamin C (ascorbic acid) content of Hayward kiwifruits (Actinidia deliciosa Planch). Food Bioprod. Process. 88, 165–173. https://doi.org/10.1016/j.fbp.2008.12.001.
- Kaymak-Ertekin, F., Gedik, A., 2005. Kinetic modelling of quality deterioration in onions during drying and storage. J. Food Eng. 68, 443–453. https://doi.org/10.1016/j. jfoodeng.2004.06.022.
- Keramat-Jahromi, M., Mohtasebi, S.S., Mousazadeh, H., Ghasemi-Varnamkhasti, M., Rahimi-Movassagh, M., 2021. Real-time moisture ratio study of drying date fruit chips based on on-line image attributes using kNN and random forest regression methods. Measurement 172, 108899. https://doi.org/10.1016/j. measurement.2020.108899.
- Khan, M.I.H., Batuwatta-Gamage, C.P., Karim, M.A., Gu, Y., 2022a. Fundamental understanding of heat and mass transfer processes for physics-informed machine learning-based drying modelling. Energies 15, 9347. https://doi.org/10.3390/ en15249347.
- Khan, M.I.H., Karim, M.A., 2017. Cellular water distribution, transport, and its investigation methods for plant-based food material. Food Res. Int. 99, 1–14.
- Khan, M.I.H., Nagy, S.A., Karim, M.A., 2018. Transport of cellular water during drying: an understanding of cell rupturing mechanism in apple tissue. Food Res. Int. 105, 772–781. https://doi.org/10.1016/j.foodres.2017.12.010.
- Khan, M.I.H., Rahman, M.M., Karim, M.A., 2020. Recent advances in micro-level experimental investigation in food drying technology. Dry. Technol. 38, 557–576. https://doi.org/10.1080/07373937.2019.1657145.
- Khan, M.I.H., Sablani, S.S., Joardder, M.U.H., Karim, M.A., 2022b. Application of machine learning-based approach in food drying: opportunities and challenges. Dry. Technol. 40, 1051–1067. https://doi.org/10.1080/07373937.2020.1853152.
- Kharaghani, A., Le, K.H., Tran, T.T.H., Tsotsas, E., 2019. Reaction engineering approach for modeling single wood particle drying at elevated air temperature. Chem. Eng. Sci. 199, 602–612. https://doi.org/10.1016/j.ces.2019.01.042.

- Kheto, A., Dhua, S., Nema, P.K., Sharanagat, V.S., 2021. Influence of drying temperature on quality attributes of bell pepper (Capsicum annuum L.): drying kinetics and modeling, rehydration, color, and antioxidant analysis. J. Food Process. Eng. 44, e13880
- Khushbu, S., Yashini, M., Rawson, A., Sunil, C., 2022. Recent advances in terahertz time-domain spectroscopy and imaging techniques for automation in agriculture and food sector. Food Anal. Methods 15, 498–526. https://doi.org/10.1007/s12161-021-02132-v.
- Kiani, S., Minaei, S., Ghasemi-Varnamkhasti, M., 2018. Real-time aroma monitoring of mint (Mentha spicata L.) leaves during the drying process using electronic nose system. Measurement 124, 447–452. https://doi.org/10.1016/j. measurement.2018.03.033.
- Kian-Pour, N., Karatas, S., 2019. Impact of different geometric shapes on drying kinetics and textural characteristics of apples at temperatures above 100 °C. Heat Mass Tran. 55, 3721–3732. https://doi.org/10.1007/s00231-019-02691-1.
- Kittibunchakul, S., Temviriyanukul, P., Chaikham, P., Kemsawasd, V., 2023. Effects of freeze drying and convective hot-air drying on predominant bioactive compounds, antioxidant potential and safe consumption of maoberry fruits. LWT 184, 114992. https://doi.org/10.1016/j.lwt.2023.114992.
- Kowalski, S.J., Rybicki, A., Rajewska, K., 2013. Optimal control of convective drying of saturated porous materials. AIChE J. 59, 4846–4857.
- Kritzinger, W., Karner, M., Traar, G., Henjes, J., Sihn, W., 2018. Digital Twin in manufacturing: a categorical literature review and classification. IFAC-PapersOnLine 51, 1016–1022. https://doi.org/10.1016/j.ifacol.2018.08.474.
- Kumar, Y., Singh, L., Sharanagat, V.S., Mani, S., Kumar, S., Kumar, A., 2021. Quality attributes of convective hot air dried spine gourd (Momordica dioica Roxb. Ex Willd) slices. Food Chem. 347, 129041. https://doi.org/10.1016/j.foodchem.2021.129041.
- Lammens, J., Goudarzi, N.M., Leys, L., Nuytten, G., van Bockstal, P.-J., Vervaet, C., Boone, M.N., Beer, T. de, 2021. Spin freezing and its impact on pore size, tortuosity and solid state. Pharmaceutics 13. https://doi.org/10.3390/pharmaceutics13122126.
- Lara-Cisneros, G., Dochain, D., 2018. Software sensor for online estimation of the VFA's concentration in anaerobic digestion processes via a high-order sliding mode observer. Ind. Eng. Chem. Res. 57, 14173–14181.
- Lewis, W.K., 1921. The rate of drying of solid materials. J. Ind. Eng. Chem. 13, 427–432. https://doi.org/10.1021/ie50137a021.
- Li, C., Yu, X., Chen, Z., Song, Q., Xu, Y., 2021a. Free space traveling-standing wave attenuation method for microwave sensing of grain moisture content. Measurement and Control 54, 336–345. https://doi.org/10.1177/0020294020962138.
- Li, L., Zhang, M., Yang, P., 2019. Suitability of LF-NMR to analysis water state and predict dielectric properties of Chinese yam during microwave vacuum drying. LWT 105, 257–264. https://doi.org/10.1016/j.lwt.2019.02.017.
- Li, M., Chen, Y., Geng, Y., Liu, F., Guo, L., Wang, X., 2021b. Convenient use of low field nuclear magnetic resonance to determine the drying kinetics and predict the quality properties of mulberries dried in hot-blast air. LWT 137, 110402. https://doi.org/ 10.1016/j.lwt.2020.110402.
- Li, Q., Lei, T., Sun, D.-W., 2023. Analysis and detection using novel terahertz spectroscopy technique in dietary carbohydrate-related research: principles and application advances. Crit. Rev. Food Sci. Nutr. 1–13. https://doi.org/10.1080/ 10408398 2023 2165032
- Lin, X., Sun, D.-W., 2022. Development of a general model for monitoring moisture distribution of four vegetables undergoing microwave-vacuum drying by hyperspectral imaging. Dry. Technol. 40, 1478–1492.
- Lin, Y., Yang, W., Wu, Z., Wang, H., 2022. Monitoring of high-moisture content particle drying in a fluidized bed by microwave and capacitance tomographic sensors. Dry. Technol. 40, 1153–1167. https://doi.org/10.1080/07373937.2020.1861005.
- Liu, J., Qiu, S., Wei, Z., 2022. Real-time measurement of moisture content of paddy rice based on microstrip microwave sensor assisted by machine learning strategies. Chemosensors 10, 376. https://doi.org/10.3390/chemosensors10100376.
- Liu, X., Chen, X., Wu, W., Zhang, Y., 2006. Process control based on principal component analysis for maize drying. Food Control 17, 894–899. https://doi.org/10.1016/j. foodcont.2005.06.008.
- Liu, Y., Zeng, Y., Hu, R., Sun, X., 2019a. Effect of contact ultrasonic power on moisture migration during far-infrared radiation drying of kiwifruit. J. Food Process. Eng. 42, e13235
- Liu, Z.-L., Bai, J.-W., Yang, W.-X., Wang, J., Deng, L.-Z., Yu, X.-L., Zheng, Z.-A., Gao, Z.-J., Xiao, H.-W., 2019b. Effect of high-humidity hot air impingement blanching (HHAIB) and drying parameters on drying characteristics and quality of broccoli florets. Dry. Technol. 37, 1251–1264. https://doi.org/10.1080/07373937.2018.1494185.
- Liu, Z.-L., Xie, L., Zielinska, M., Pan, Z., Wang, J., Deng, L.-Z., Wang, H., Xiao, H.-W., 2021. Pulsed vacuum drying enhances drying of blueberry by altering micro-, ultrastructure and water status and distribution. LWT 142, 111013. https://doi.org/ 10.1016/i.lwt.2021.111013.
- Long, J., Yang, J., Peng, J., Pan, L., Tu, K., 2021. Detection of moisture and carotenoid content in carrot slices during hot air drying based on multispectral imaging equipment with selected wavelengths. Int. J. Food Eng. 17, 727–735. https://doi. org/10.1515/jife-2021-0127.
- López, J., Uribe, E., Vega-Gálvez, A., Miranda, M., Vergara, J., Gonzalez, E., Di Scala, K., 2010. Effect of air temperature on drying kinetics, vitamin C, antioxidant activity, total phenolic content, non-enzymatic browning and firmness of blueberries variety O Neil. Food Bioprocess Technol. 3, 772–777.
- Lu, J., Wang, X., Zhang, C., Ma, Y., Zhao, X., 2015. Effect of drying temperature on qualities of mint. In: International Conference on Advanced Engineering Materials and Technology. Atlantis Press, pp. 958–962.

- Lu, X., Tsotsas, E., Kharaghani, A., 2021. Drying of capillary porous media simulated by coupling of continuum-scale and micro-scale models. Int. J. Multiphas. Flow 140, 103654
- Luning, P.A., Ebbenhorst-Seller, T., Rijk, T. de, Roozen, J.P., 1995. Effect of hot-air drying on flavour compounds of bell peppers (Capsicum annuum). J. Sci. Food Agric. 68, 355–365.
- Mahayothee, B., Komonsing, N., Khuwijitjaru, P., Nagle, M., Müller, J., 2019. Influence of drying conditions on colour, betacyanin content and antioxidant capacities in dried red-fleshed dragon fruit (Hylocereus polyrhizus). Int. J. Food Sci. Technol. 54, 440, 470
- Makarichian, A., Amiri Chayjan, R., Ahmadi, E., Mohtasebi, S.S., 2021. Assessment the influence of different drying methods and pre-storage periods on garlic (Allium Sativum L.) aroma using electronic nose. Food Bioprod. Process. 127, 198–211. https://doi.org/10.1016/j.fbp.2021.02.016.
- Martynenko, A., 2017. Computer vision for real-time control in drying. Food Eng. Rev. 9, 91–111. https://doi.org/10.1007/s12393-017-9159-5.
- Martynenko, A., Misra, N.N., 2020. Machine learning in drying. Dry. Technol. 38, 596–609.
- Martynenko, A.I., 2006. Computer-vision system for control of drying processes. Dry. Technol. 24, 879–888. https://doi.org/10.1080/07373930600734067.
- Martynenko, A.I., Yang, S.X., 2007. An intelligent control system for thermal processing of biomaterials. In: 2007 IEEE International Conference on Networking, Sensing and Control
- Massei, A., Falco, N., Fissore, D., 2025. NIR-based real-time monitoring of freeze-drying processes: application to fault and endpoint detection. Processes 13, 452.
- Matys, A., Witrowa-Rajchert, D., Parniakov, O., Wiktor, A., 2023. Assessment of the effect of air humidity and temperature on convective drying of apple with pulsed electric field pretreatment. LWT 188, 115455. https://doi.org/10.1016/j. lwt.2023.115455.
- Md Saleh, R., Kulig, B., Arefi, A., Hensel, O., Sturm, B., 2022. Prediction of total carotenoids, color, and moisture content of carrot slices during hot air drying using non-invasive hyperspectral imaging technique. J. Food Process. Preserv. 46, e16460.
- Méndez-Lagunas, L., Rodríguez-Ramírez, J., Cruz-Gracida, M., Sandoval-Torres, S., Barriada-Bernal, G., 2017. Convective drying kinetics of strawberry (Fragaria ananassa): effects on antioxidant activity, anthocyanins and total phenolic content. Food Chem. 230, 174–181.
- Midilli, A., Kucuk, H., Yapar, Z., 2002. A new model for single-layer drying. Dry. Technol. 20, 1503–1513. https://doi.org/10.1081/DRT-120005864.
- Mishra, S., Sanwal, N., Sharma, N., Sahu, J.K., 2022. Multivariate analysis of chemometric based aroma dynamics in small cardamom (Elettaria cardamomum Maton) during drying. J. Food Sci. Technol. 59, 4761–4771.
- Mokhtar, S., Morsy, N., 2014. Effect of hot air drying variables on phytochemicals and antioxidant capacity of Jew's mallow (Corchorus olitorius L.) leaves. Suez Canal University Journal of Food Sciences 2, 1–8.
- Moscetti, R., Nallan Chakravartula, S.S., Bandiera, A., Bedini, G., Massantini, R., 2020. Computer vision technology for quality monitoring in smart drying system. In: 2020 IEEE International Workshop on Metrology for Agriculture and Forestry (MetroAgriFor). 2020 IEEE International Workshop on Metrology for Agriculture and Forestry (MetroAgriFor), Trento, Italy. 11/4/2020 - 11/6/2020. IEEE, pp. 134-138.
- Mousakhani-Ganjeh, A., Amiri, A., Nasrollahzadeh, F., Wiktor, A., Nilghaz, A., Pratap-Singh, A., Mousavi Khaneghah, A., 2021. Electro-based technologies in food drying a comprehensive review. LWT 145, 111315. https://doi.org/10.1016/j.lwt.2021.111315.
- Mujaffar, S., John, S., 2018. Thin-layer drying behavior of West Indian lemongrass (Cymbopogan citratus) leaves. Food Sci. Nutr. 6, 1085–1099.
- Nagvanshi, S., Venkata, S.K., Goswami, T.K., 2021. Study of color kinetics of banana (Musa cavendish) under microwave drying by application of image analysis. Food Sci. Technol. Int. 27, 660–673. https://doi.org/10.1177/1082013220981334.
- Nakagawa, K., Tamiya, S., Sakamoto, S., Do, G., Kono, S., 2018. Observation of microstructure formation during freeze-drying of dextrin solution by in-situ X-ray computed tomography. Front. Chem. 6, 418. https://doi.org/10.3389/ fchem.2018.00418.
- Ndisya, J., Gitau, A., Mbuge, D., Arefi, A., Bădulescu, L., Pawelzik, E., Hensel, O., Sturm, B., 2021. Vis-NIR hyperspectral imaging for online quality evaluation during food processing: a case study of hot air drying of purple-speckled cocoyam (Colocasia esculenta (L.) schott). Processes 9, 1804.
- Ndisya, J., Mbuge, D., Kulig, B., Gitau, A., Hensel, O., Sturm, B., 2020. Hot air drying of purple-speckled Cocoyam (Colocasia esculenta (L.) Schott) slices: optimisation of drying conditions for improved product quality and energy savings. Therm. Sci. Eng. Prog. 18, 100557. https://doi.org/10.1016/j.tsep.2020.100557.
- Nurkhoeriyati, T., Arefi, A., Kulig, B., Sturm, B., Hensel, O., 2023. Non-destructive monitoring of quality attributes kinetics during the drying process: a case study of celeriac slices and the model generalisation in selected commodities. Food Chem. 424, 136379.
- Ojediran, J.O., Okonkwo, C.E., Adeyi, A.J., Adeyi, O., Olaniran, A.F., George, N.E., Olayanju, A.T., 2020. Drying characteristics of yam slices (Dioscorea rotundata) in a convective hot air dryer: application of ANFIS in the prediction of drying kinetics. Heliyon 6, e03555.
- Ojediran, J.O., Okonkwo, C.E., Olaniran, A.F., Iranloye, Y.M., Adewumi, A.D., Erinle, O., Afolabi, Y.T., Adeyi, O., Adeyi, A., 2021. Hot air convective drying of hog plum fruit (Spondias mombin): effects of physical and edible-oil-aided chemical pretreatments on drying and quality characteristics. Heliyon 7, e08312.
- Oliveira-Silva, E., Prada, C. de, Navia, D., 2021. Dynamic optimization integrating modifier adaptation using transient measurements. Comput. Chem. Eng. 149, 107282.

- Olmos, A., Trelea, I.-C., Courtois, F., Bonazzi, C., Trystram, G., 2002. Dynamic optimal control of batch rice drying process. Dry. Technol. 20, 1319–1345.
- Omolola, A.O., Jideani, A.I.O., Kapila, P.F., 2014. Modeling microwave drying kinetics and moisture diffusivity of Mabonde banana variety. Int. J. Agric. Biol. Eng. 7, 107–113
- Onwude, D.I., Hashim, N., Abdan, K., Janius, R., Chen, G., 2018a. Combination of computer vision and backscattering imaging for predicting the moisture content and colour changes of sweet potato (Ipomoea batatas L.) during drying. Comput. Electron. Agric. 150, 178–187. https://doi.org/10.1016/j.compag.2018.04.015.
- Onwude, D.I., Hashim, N., Abdan, K., Janius, R., Chen, G., Kumar, C., 2018b. Modelling of coupled heat and mass transfer for combined infrared and hot-air drying of sweet potato. J. Food Eng. 228, 12–24.
- Ouyang, M., Huang, Y., Wang, Y., Luo, F., Liao, L., 2022. Stability of carotenoids and carotenoid esters in pumpkin (Cucurbita maxima) slices during hot air drying. Food Chem. 367, 130710. https://doi.org/10.1016/j.foodchem.2021.130710.
- Ozden, S., 2022. Computer vision application on controlling and modeling the food drying process: a case study for radish (Raphanus Sativus). In: 9th International Conference on Electrical and Electronics Engineering (ICEEE), Alanya, Turkey. 3/29/2022 3/31/2022. IEEE, pp. 151–155.
- Ozsan Kilic, T., Boyar, I., Gungor, K.K., Torun, M., Perendeci, N.A., Ertekin, C., Onus, A. N., 2023. Improvement of hot air dried bitter gourd (Momordica charantia L.) product quality: optimization of drying and blanching process by experimental design. Agriculture 13, 1849. https://doi.org/10.3390/agriculture13091849.
- Page, G.E., 1949. Factors Influencing the Maximum Rates of Air Drying Shelled Corn in Thin Layers. Purdue University
- Palmkron, S.B., Bergenståhl, B., Håkansson, S., Wahlgren, M., Fureby, A.M., Larsson, E., 2023. Quantification of structures in freeze-dried materials using X-ray microtomography. Colloids Surf. A Physicochem. Eng. Asp. 658, 130726. https:// doi.org/10.1016/j.colsurfa.2022.130726.
- Parveez Zia, M., Alibas, I., 2021. The effect of different drying techniques on color parameters, ascorbic acid content, anthocyanin and antioxidant capacities of cornelian cherry. Food Chem. 364, 130358. https://doi.org/10.1016/j. foodchem.2021.130358.
- Pei, F., Yang, W., Ma, N., Fang, Y., Zhao, L., An, X., Xin, Z., Hu, Q., 2016. Effect of the two drying approaches on the volatile profiles of button mushroom (Agaricus bisporus) by headspace GC–MS and electronic nose. LWT 72, 343–350. https://doi. org/10.1016/i.lwt.2016.05.004.
- Pitarch, J.L., Sala, A., Prada, C. de, 2019. A systematic grey-box modeling methodology via data reconciliation and SOS constrained regression. Processes 7, 170.
- Piyarach, K., Nipawan, K., Chadapon, C., Daluwan, S., Kunjana, R., 2020. Effect of drying on β-Carotene, α carotene, Lutein and Zeaxanthin content in vegetables and its application for vegetable seasoning. E3S Web of Conferences 141, 2007. https://doi. org/10.1051/e3sconf/202014102007.
- Prada, C. de, Galán-Casado, S., Pitarch, J.L., Sarabia, D., Galán, A., Gutiérrez, G., 2022. Gemelos digitales en la industria de procesos. Revista Iberoamericana de Automática e Informática industrial 19, 285–296.
- Prawiranto, K., Carmeliet, J., Defraeye, T., 2021. Physics-based digital twin identifies trade-offs between drying time, fruit quality, and energy use for solar drying. Front. Sustain. Food Syst. 4, 606845. https://doi.org/10.3389/fsufs.2020.606845.
- Preethi, R., Deotale, S.M., Moses, J.A., Anandharamakrishnan, C., 2020. Conductive hydro drying of beetroot (Beta vulgaris L) pulp: insights for natural food colorant applications. J. Food Process. Eng. 43, e13557.
- Przybyf, K., Koszela, K., 2023. Applications MLP and other methods in artificial intelligence of fruit and vegetable in convective and spray drying. Appl. Sci. 13, 2965. https://doi.org/10.3390/app13052965.
- Pu, Y.-Y., Zhao, M., O'Donnell, C., Sun, D.-W., 2018. Nondestructive quality evaluation of banana slices during microwave vacuum drying using spectral and imaging techniques. Dry. Technol. 36, 1542–1553.
- Pu, Yu Elaine, Ma, Lisa, Dear, Barton, Zhu, Aiden, Li, Jianmin, Zhang, Shawn, Shi, Weixian, 2023. Understanding the impact of microstructures on reconstitution and drying kinetics of Lyophilized cake using X-ray microscopy and image-based simulation. J. Pharmaceut. Sci. 112 (6), 1625–1634. https://doi.org/10.1016/j. xphs.2023.01.002.
- Putranto, A., Chen, X.D., Webley, P.A., 2011. Modeling of drying of food materials with thickness of several centimeters by the reaction engineering approach (REA). Dry. Technol. 29, 961–973. https://doi.org/10.1080/07373937.2011.557793.
- Qadri, O.S., Osama, K., Srivastava, A.K., 2020. Foam mat drying of papaya using microwaves: machine learning modeling. J. Food Process. Eng. 43, e13394.
- Queiroz, Nebra, S.A., 2001. Theoretical and experimental analysis of the drying kinetics of bananas. J. Food Eng. 47, 127–132.
- Quispe-Fuentes, I., Vega-Gálvez, A., Vásquez, V., Uribe, E., Astudillo, S., 2017.
 Mathematical modeling and quality properties of a dehydrated native Chilean berry.
 J. Food Process. Eng. 40, e12499. https://doi.org/10.1111/jfpe.12499.
- Rahman, M.M., Farahani, M.A., Wuest, T., 2023. Multivariate time-series classification of critical events from industrial drying hopper operations: a deep learning approach. Journal of Manufacturing and Materials Processing 7, 164. https://doi.org/10.3390/ jmmp7050164.
- Raissi, M., Yazdani, A., Karniadakis, G.E., 2020. Hidden fluid mechanics: learning velocity and pressure fields from flow visualizations. Science 367, 1026–1030.
- Rajendran, B., Sudalaimani, A., Jothi, T., Mohankumar, A., Sampathkumar, D., Mariappan, M., Mohaideen, A., 2023. Mathematical modelling, drying behavior, and quality investigation of the Turkey berry in a fluidized bed dryer. J. Food Qual. 2023.
- Ramachandran, R.P., Akbarzadeh, M., Paliwal, J., Cenkowski, S., 2018. Computational fluid dynamics in drying process modelling—a technical review. Food Bioprocess Technol. 11, 271–292.

- Raponi, F., Moscetti, R., Nallan Chakravartula, S.S., Fidaleo, M., Massantini, R., 2022. Monitoring the hot-air drying process of organically grown apples (cv. Gala) using computer vision. Biosyst. Eng. 223, 1–13. https://doi.org/10.1016/j.biosystemseng.2021.07.005.
- Ren, Y., Lei, T., Sun, D.-W., 2023. In-situ indirect measurements of real-time moisture contents during microwave vacuum drying of beef and carrot slices using Terahertz time-domain spectroscopy. Food Chem., 135943 https://doi.org/10.1016/j. foodchem.2023.135943.
- Ren, Y., Sun, D.-W., 2022. Advanced application of terahertz time-domain spectral technique for In-situ monitoring of microwave vacuum dehydration. In: 2022 Houston, Texas July 17-20, 2022. 2022 Houston, Texas July 17-20, 2022. American Society of Agricultural and Biological Engineers, St. Joseph, MI.
- Ritto, T.G., Rochinha, F.A., 2021. Digital twin, physics-based model, and machine learning applied to damage detection in structures. Mech. Syst. Signal Process. 155, 107614.
- Rodríguez, K., Ah-Hen, K.S., Vega-Gálvez, A., Vásquez, V., Quispe-Fuentes, I., Rojas, P., Lemus-Mondaca, R., 2016. Changes in bioactive components and antioxidant capacity of maqui, Aristotelia chilensis [Mol] Stuntz, berries during drying. LWT 65, 537–542. https://doi.org/10.1016/j.lwt.2015.08.050.
- Romano, G., Baranyai, L., Gottschalk, K., Zude, M., 2008. An approach for monitoring the moisture content changes of drying banana slices with laser light backscattering imaging. Food Bioprocess Technol. 1, 410–414. https://doi.org/10.1007/s11947-008-0113-7
- Sabat, M., Kotwaliwale, N., Chakraborty, S.K., Kumar, M., 2022. Long short-term memory based real-time monitoring of potato slice drying using image chromatic features. J. Food Process. Preserv. 46. https://doi.org/10.1111/jfpp.17232.
- Sadaka, S., 2022. Impact of grain layer thickness on rough rice drying kinetics parameters. Case Stud. Therm. Eng. 35, 102026. https://doi.org/10.1016/j csite.2022.102026.
- Saha, B., Bucknall, M.P., Arcot, J., Driscoll, R., 2018. Profile changes in banana flavour volatiles during low temperature drying. Food Res. Int. 106, 992–998.
- Sahoo, M., Titikshya, S., Aradwad, P., Kumar, V., Naik, S.N., 2022. Study of the drying behaviour and color kinetics of convective drying of yam (Dioscorea hispida) slices. Ind. Crop. Prod. 176, 114258.
- Sarkar, A., Hossain, M.W., Alam, M., Biswas, R., Roy, M., Haque, M.I., 2023. Drying conditions and varietal impacts on physicochemical, antioxidant and functional properties of onion powder. J. Agric. Food Res. 12, 100578.
- Sarpong, F., Rashid, M.T., Wahia, H., Aly, T.A.-G.A., Zhou, C., 2021. Mitigation of relative humidity (RH) on phytochemicals and functional groups of dried pineapple (Ananas comosus) slices. Int. J. Food Eng. 17, 265–274. https://doi.org/10.1515/ iife-2020-0190.
- Sasikumar, R., Mangang, I.B., Vivek, K., Jaiswal, A.K., 2023. Effect of ultrasound-assisted thin bed drying for retaining the quality of red bell pepper and compare the predictive ability of the mathematical model with artificial neural network. J. Food Process. Eng. 46, e14468.
- Schemminger, J., Raut, S., Sturm, B., Defraeye, T., 2024. A hybrid digital shadow to assess biological variability in carrot slices during drying. Therm. Sci. Eng. Prog. 50, 102507. https://doi.org/10.1016/j.tsep.2024.102507.
- Sebben, J.A., Da Silveira Espindola, J., Ranzan, L., Fernandes de Moura, N., Trierweiler, L.F., Trierweiler, J.O., 2018. Development of a quantitative approach using Raman spectroscopy for carotenoids determination in processed sweet potato. Food Chem. 245, 1224–1231. https://doi.org/10.1016/j.foodchem.2017.11.086. Sehrawat, R., Nema, P.K., Kaur, B.P., 2018. Quality evaluation and drying characteristics
- Sehrawat, R., Nema, P.K., Kaur, B.P., 2018. Quality evaluation and drying characteristics of mango cubes dried using low-pressure superheated steam, vacuum and hot air drying methods. LWT 92, 548–555. https://doi.org/10.1016/j.lwt.2018.03.012.
- Sharma, S., Dhalsamant, K., Tripathy, P.P., 2019. Application of computer vision technique for physical quality monitoring of turmeric slices during direct solar drying. J. Food Meas. Char. 13, 545–558. https://doi.org/10.1007/s11694-018-9968-0.
- Shi, X., Yang, Y., Li, Z., Wang, X., Liu, Y., 2020. Moisture transfer and microstructure change of banana slices during contact ultrasound strengthened far-infrared radiation drying. Innov. Food Sci. Emerg. Technol. 66, 102537. https://doi.org/ 10.1016/j.ifset.2020.102537.
- Shrestha, L., Crichton, S.O.J., Kulig, B., Kiesel, B., Hensel, O., Sturm, B., 2020.
 Comparative analysis of methods and model prediction performance evaluation for continuous online non-invasive quality assessment during drying of apples from two cultivars. Therm. Sci. Eng. Prog. 18, 100461.
- Siebert, T., Zuber, M., Engelhardt, S., Baumbach, T., Karbstein, H.P., Gaukel, V., 2018. Visualization of crust formation during hot-air-drying via micro-CT. Dry. Technol.
- Simonič, M., Klančnik, S., 2024. Predicting Corn Moisture Content in Continuous Drying Systems Using LSTM Neural Networks.
- Siyum, Z.H., Pham, T.T., Vozáry, E., Kaszab, T., Le Nguyen, L.P., Baranyai, L., 2023. Monitoring of banana's optical properties by laser light backscattering imaging technique during drying. J. Food Meas. Char. 17, 5268–5287. https://doi.org/ 10.1007/s11694-023-02019-y.
- Song, Q., Wei, X., Sun, W., Li, D., 2022. Model predictive control strategy of head rice yield in paddy rice intermittent drying. Dry. Technol. 40, 2941–2951. https://doi. org/10.1080/07373937.2021.1979032.
- Stamenković, Z., Pavkov, I., Radojčin, M., Tepić Horecki, A., Kešelj, K., Bursać Kovačević, D., Putnik, P., 2019. Convective drying of fresh and frozen raspberries and change of their physical and nutritive properties. Foods 8, 251.
- Sturm, B., 2010. Einfluss Der Führung Des Trocknungsprozesses Auf Den Trocknungsverlauf Und Die Produkteigenschaften Empfindlicher Biologischer Güter.
- Sturm, B., 2018. Systemic optimisation and design approach for thermal food processesincrease of quality, process-and resource efficiency in dried agricultural products manutacturing. Habilitationsschrift. Kassel-Germany.

- Sturm, B., Hofacker, W., 2007. On the improvement of dried agricultural products via active temperature control. In: 18th DAAAM Symposium on Intelligent Manufacturing & Automation. Newcastle University.
- Sturm, B., Hofacker, W., Hensel, O., 2009. Automatic control of the drying process of biological materials using optical sensors to acquire surface temperature, color and shape. In: ASABE, 2009 Reno, Nevada, June 21-June 24, 2009.
- Sturm, B., Hofacker, W.C., 2010. Control strategies for stepwise drying of agricultural products. In: 17th International Drying Symposium. Newcastle University.
- Sturm, B., Moscetti, R., Crichton, S., Raut, S., Bantle, M., Massantini, R., 2018. Feasibility of Vis/NIR spectroscopy and image analysis as basis of the development of smart-drying technologies. In: Proceedings of 21th International Drying Symposium. 21st International Drying Symposium. 9/11/2018 9/14/2018. Universitat Politècnica València. Valencia.
- Su, W.-H., Bakalis, S., Sun, D.-W., 2020. Chemometric determination of time series moisture in both potato and sweet potato tubers during hot air and microwave drying using near/mid-infrared (NIR/MIR) hyperspectral techniques. Dry. Technol. 38, 806–823. https://doi.org/10.1080/07373937.2019.1593192.
- Sufer, O., Palazoglu, T.K., 2019. A study on hot-air drying of pomegranate. J. Therm. Anal. Calorim. 137, 1981–1991.
- Sujinda, N., Varith, J., Shamsudin, R., Jaturonglumlert, S., Chamnan, S., 2021.
 Development of a closed-loop control system for microwave freeze-drying of carrot slices using a dynamic microwave logic control. J. Food Eng. 302, 110559. https://doi.org/10.1016/j.jfoodeng.2021.110559.
- Sun, Q., Zhang, M., Mujumdar, A.S., 2019a. Recent developments of artificial intelligence in drying of fresh food: a review. Crit. Rev. Food Sci. Nutr. 59, 2258–2275
- Sun, Q., Zhang, M., Mujumdar, A.S., 2021a. Evaluation of potential application of artificial intelligent control aided by LF-NMR in drying of carrot as model material. Dry. Technol. 39, 1149–1157. https://doi.org/10.1080/07373937.2020.1743999.
- Sun, Q., Zhang, M., Mujumdar, A.S., Yang, P., 2019b. Combined LF-NMR and artificial intelligence for continuous real-time monitoring of carrot in microwave vacuum drying. Food Bioprocess Technol. 12, 551–562. https://doi.org/10.1007/s11947-018-2231-1.
- Sun, Q., Zhang, M., Yang, P., 2019c. Combination of LF-NMR and BP-ANN to monitor water states of typical fruits and vegetables during microwave vacuum drying. LWT 116, 108548. https://doi.org/10.1016/j.lwt.2019.108548.
- Sun, Y., Zhang, M., Bhandari, B., Yang, P., 2019d. Intelligent detection of flavor changes in ginger during microwave vacuum drying based on LF-NMR. Food Res. Int. 119, 417–425. https://doi.org/10.1016/j.foodres.2019.02.019.
- Sun, Y., Zhang, M., Ju, R., Mujumdar, A., 2021b. Novel nondestructive NMR method aided by artificial neural network for monitoring the flavor changes of garlic by drying. Dry. Technol. 39, 1184–1195. https://doi.org/10.1080/ 07373937.2020.1821211.
- Sun, Y., Zhang, M., Mujumdar, A.S., Yu, D., 2021c. Pulse-spouted microwave freeze drying of raspberry: control of moisture using ANN model aided by LF-NMR. J. Food
- Eng. 292, 110354. https://doi.org/10.1016/j.jfoodeng.2020.110354.

 Tan, S., Miao, Y., Zhou, C., Luo, Y., Lin, Z., Xie, R., Li, W., 2022. Effects of hot air drying on drying kinetics and anthocyanin degradation of blood-flesh peach. Foods 11, 1596.
- Tayyab, M., Sturm, B., Delele, M.A., Arefi, A., 2025. Hyperspectral and 3D point cloud imaging unraveling of physio-chemical shifts during drying of purple carrot and golden kiwifruit. Food Control, 111578. https://doi.org/10.1016/j. foodcont 2025 111578
- Tekgül, Y., Erten, E.S., 2022. Quality properties and headspace volatiles of hot air-dried strawberries. An Acad. Bras Ciências 94, e20201277.
- Tepe, F.B., Tepe, T.K., Ekinci, A., 2022. Impact of air temperature on drying characteristics and some bioactive properties of kiwi fruit slices. Chem. Ind. Chem. Eng. O.
- Thuy, N.M., Le Hiep, H., van Tai, N., Huong, H.T.T., Minh, V.Q., 2022. Impact of drying temperatures on drying behaviours, energy consumption and quality of purple sweet potato flour. Acta Scientiarum Polonorum Technologia Alimentaria 21, 379–387.
- Trelea, I.-C., Trystram, G., Courtois, F., 1997. Optimal constrained non-linear control of batch processes: application to corn drying. J. Food Eng. 31, 403–421.
- Trelea, I.C., Trystram, G., Courtois, F., 1999. Influence of model uncertainty on the dynamic optimal control performance of a batch corn drying process. Dry. Technol. 17, 1173–1180.
- Tzempelikos, D.A., Mitrakos, D., Vouros, A.P., Bardakas, A.V., Filios, A.E., Margaris, D.P., 2015. Numerical modeling of heat and mass transfer during convective drying of cylindrical quince slices. J. Food Eng. 156, 10–21.
- Vanbillemont, B., Lammens, J., Goethals, W., Vervaet, C., Boone, M.N., Beer, T. de, 2020. 4D micro-computed X-ray tomography as a tool to determine critical process and product information of spin freeze-dried unit doses. Pharmaceutics 12. https://doi.org/10.3390/pharmaceutics12050430.
- Vega, A.-M.N., Sturm, B., Hofacker, W., 2016. Simulation of the convective drying process with automatic control of surface temperature. J. Food Eng. 170, 16–23.
- Verboven, Pieter, Defraeye, Thijs, Datta, Ashim K., Nicolai, Bart, 2020. Digital twins of food process operations: the next step for food process models? Curr. Opin. Food Sci. 35, 79–87. https://doi.org/10.1016/j.cofs.2020.03.002.

- Verma, L.R., Bucklin, R.A., Endan, J.B., Wratten, F.T., 1985. Effects of drying air parameters on rice drying models. Transactions of the ASAE 28, 296–301. https:// doi.org/10.13031/2013.32245.
- Voda, A., Homan, N., Witek, M., Duijster, A., van Dalen, G., van der Sman, R., Nijsse, J., van Vliet, L., van As, H., van Duynhoven, J., 2012. The impact of freeze-drying on microstructure and rehydration properties of carrot. Food Res. Int. 49, 687–693. https://doi.org/10.1016/j.foodres.2012.08.019.
- Walker, G.M., Bell, S.E., Greene, K., Jones, D.S., Andrews, G.P., 2009. Characterisation of fluidised bed granulation processes using in-situ raman spectroscopy. Chem. Eng. Sci. 64, 91–98.
- Wang, J., Wu, G., Wang, Z., Shu, B., Li, L., Zhang, R., Huang, F., Dong, L., Zhang, M., Chen, S., 2020. The influence of processing conditions on kinetics, anthocyanin profile and antioxidant activity of purple sweet potato subjected to hot air drying. J. Food Process. Eng. 43, e13472.
- Welsh, Z.G., Khan, M.I.H., Karim, M.A., 2021. Multiscale modeling for food drying: a homogenized diffusion approach. J. Food Eng. 292, 110252.
- Wen, Y.-X., Chen, L.-Y., Li, B.-S., Ruan, Z., Pan, Q., 2020. Effect of infrared radiation-hot air (IR-HA) drying on kinetics and quality changes of star anise (Illicium verum). Dry. Technol. 39, 90–103. https://doi.org/10.1080/07373937.2019.1696816.
- Wongrat, W., Younes, A., Elkamel, A., Douglas, P.L., Lohi, A., 2011. Control vector optimization and genetic algorithms for mixed-integer dynamic optimization in the synthesis of rice drying processes. J. Franklin Inst. 348, 1318–1338.
- Xi, H., Zhu, A., Klinzing, G.R., Zhou, L., Zhang, S., Gmitter, A.J., Ploeger, K., Sundararajan, P., Mahjour, M., Xu, W., 2020. Characterization of spray dried particles through microstructural imaging. J. Pharmaceut. Sci. 109, 3404–3412. https://doi.org/10.1016/j.xphs.2020.07.032.
- Xie, C., Li, X., Nie, P., He, Y., 2013. Application of time series hyperspectral imaging (TS-HSI) for determining water content within tea leaves during drying. Transactions of the ASABE 56, 1431–1440.
- Xu, Y., Liu, W., Li, L., Cao, W., Zhao, M., Dong, J., Ren, G., Bhandari, B., Duan, X., 2022. Dynamic changes of non-volatile compounds and evaluation on umami during infrared assisted spouted bed drying of shiitake mushrooms. Food Control 142, 100245
- Yaldiz, O., Ertekin, C., Uzun, H., 2001. Mathematical modeling of thin layer solar drying of sultana grapes. Energy 26, 457–465. https://doi.org/10.1016/S0360-5442(01) 00018-4.
- Yang, S., Liu, T., Fu, N., Xiao, J., Putranto, A., Chen, X.D., 2021. Convective drying of highly shrinkable vegetables: new method on obtaining the parameters of the reaction engineering approach (REA) framework. J. Food Eng. 305, 110613.
- Yang, Y., Chen, J., Jiang, Y., Qian, M.C., Deng, Y., Xie, J., Li, J., Wang, J., Dong, C., Yuan, H., 2022. Aroma dynamic characteristics during the drying process of green tea by gas phase electronic nose and gas chromatography-ion mobility spectrometry. LWT 154, 112691. https://doi.org/10.1016/j.lwt.2021.112691.
- Younas, S., Mao, Y., Liu, C., Murtaza, M.A., Ali, Z., Wei, L., Liu, W., Zheng, L., 2021. Measurement of water fractions in freeze-dried shiitake mushroom by means of multispectral imaging (MSI) and low-field nuclear magnetic resonance (LF-NMR). J. Food Compos. Anal. 96. 103694. https://doi.org/10.1016/j.ifca.2020.103694.
- Yu, P., Huang, M., Zhang, M., Zhu, Q., Qin, J., 2020. Rapid detection of moisture content and shrinkage ratio of dried carrot slices by using a multispectral imaging system. Infrared Phys. Technol. 108, 103361. https://doi.org/10.1016/j. infrared.2020.103361.
- Zhang, H., Peng, J., Zhang, Y., Liu, Q., Pan, L., Tu, K., 2020. Discrimination of volatiles of shiitakes (Lentinula edodes) produced during drying process by electronic nose. Int. J. Food Eng. 16. https://doi.org/10.1515/ijfe-2019-0233.
- Zhang, J., Cao, J., Pei, Z., Wei, P., Xiang, D., Cao, X., Shen, X., Li, C., 2019. Volatile flavour components and the mechanisms underlying their production in golden pompano (Trachinotus blochii) fillets subjected to different drying methods: a comparative study using an electronic nose, an electronic tongue and SDE-GC-MS. Food Res. Int. 123, 217–225. https://doi.org/10.1016/j.foodres.2019.04.069.
- Zhang, L., Dong, X., Feng, X., Ibrahim, S.A., Huang, W., Liu, Y., 2021a. Effects of drying process on the volatile and non-volatile flavor compounds of lentinula edodes. Foods 10. https://doi.org/10.3390/foods10112836.
- Zhang, L., Yu, X., Arun S, M., Zhou, C., 2022. Effect of freeze-thaw pretreatment combined with variable temperature on infrared and convection drying of lotus root. LWT 154, 112804. https://doi.org/10.1016/j.lwt.2021.112804.
- Zhang, L., Zhang, M., Mujumdar, A.S., 2021b. Terahertz spectroscopy: a powerful technique for food drying research. Food Rev. Int. 1–18. https://doi.org/10.1080/ 87559129 2021 1936004
- Zhou, H., Huang, M., Zhu, Q., Zhang, M., 2022. Developing C-LSTM model for evaluating moisture content of carrot slices during drying. Dry. Technol. 40, 2964–2974. https://doi.org/10.1080/07373937.2021.1983822.
- Zhu, Y., Ju, R., Ma, F., Qian, J., Yan, J., Li, S., Li, Z., 2021. Moisture variation analysis of the green plum during the drying process based on low-field nuclear magnetic resonance. J. Food Sci. 86, 5137–5147.
- Zia, M.P., Alibas, I., 2021. Influence of the drying methods on color, vitamin C, anthocyanin, phenolic compounds, antioxidant activity, and in vitro bioaccessibility of blueberry fruits. Food Biosci. 42, 101179. https://doi.org/10.1016/j.fbio.2021.101179.